

**Orbitally excited hadrons**

I. Yu. Kobzarev, B. V. Martem'yanov, and M. G. Shchepkin

*Institute of Theoretical and Experimental Physics, Moscow*

(Submitted 16 January 1991; resubmitted after revision 12 December 1991)

Usp. Fiz. Nauk. **162**, 1-41 (April 1992)

This review is devoted to the description of high-spin hadrons. A relativistic QCD-string model that reproduces the principal feature of the spectra of orbitally excited hadrons, namely, the linearity of Regge trajectories, is employed. Particular emphasis is placed on the inclusion of spin effects. For large orbital excitations, these effects appear as the spin-orbit interaction whose sign and magnitude are determined by confinement properties. Arguments are presented in support of the proposition that, for large orbital excitations, the spin-orbit interaction of quarks in the string model is largely due to the Thomas effect. The consequences of this hypothesis are analyzed phenomenologically, and the results are compared with experimental data. Specific predictions are obtained and await experimental verification. Orbital excitations of four-quark and dibaryon states are predicted.

**INTRODUCTION**

We present a review of the quasiclassical approach to the spectroscopy of high-spin hadrons, taking as our starting point the hypothesis that such hadrons are orbitally excited analogs of the 'ordinary' light hadrons  $\rho$ ,  $\pi$ ,  $N$ , and so on. We also examine the characteristic properties of orbital excitations of hadrons containing heavy quarks.

One of the central questions that we analyze in detail is that of the effects of the quark spin. For large orbital excitations, spin effects appear as the spin-orbit interaction whose sign and magnitude are determined by the structure of the interaction responsible for the confinement of quarks. A relatively clear picture emerges when the quasiclassical approximation is used to calculate dynamic variables, but, of course, this approach restricts the analysis to large orbital excitations.

A relatively large number of mesons and baryons with high spins has now been identified experimentally.<sup>1</sup> On the other hand, existing spectroscopic data do not as yet provide unambiguous evidence for spin-orbit effects. This will require, for example, the masses of particles on  $\pi$ -trajectories with spins  $J > 3$ .

It has been established experimentally that the Regge trajectories are linear to a good approximation. This imposes relatively stringent restrictions on the choice of the rotator model capable of providing a reasonable description of real high-spin hadrons. Actually, the linearity of the trajectory means that the mass difference  $\Delta M$  between neighboring particles on a given trajectory decreases with increasing  $J$  as  $1/J^{1/2} \sim 1/M$ . We know that, in the quasiclassical description, the separation between neighboring rotational levels is equal to the rotational frequency  $\omega$ . This frequency decreases as  $\omega \sim 1/J^{1/2}$  and, at the same time, the energy (mass) of the rotator is  $M \sim J^{1/2}$ , so that the energy can be increased by increasing the size of the rotator. Moreover, the quasiclassical approach must be relativistic, since we are discussing orbital excitations of hadron states with masses exceeding the effective quark masses.

The relativistic model of a string under constant tension  $\nu$  can account for these properties. In the simplest string model (the Nambu model<sup>2</sup>), the string is assumed to be straight and the quarks massless. The model predicts linear Regge trajectories

$$J = \frac{1}{2\pi\nu} M^2$$

We have already noted that the spins of quarks localized at the ends of the string must be taken into account in applications involving real hadrons, which leads to the problem of evaluation of the spin-orbit interaction energy in the string model. Before this can be done, the string itself has to be specified in some way.

The dual superconducting string model<sup>3</sup> has been widely discussed in the literature. It rests on the assumption that the linear energy density of the string,  $\nu$ , is related to (a) the gluoelectric field connecting color charges at the ends of the string and (b) the destruction of the QCD vacuum by this field. The model can be specified in greater detail, which leads to the concept of a tube of force of the gluoelectric field, screened by a current of topological monopoles.<sup>3</sup> When this approach is adopted, and the thin-string approximation is employed, we find that, in the reference frame in which the quarks are at rest, they experience only the electric field<sup>4</sup> that has no interaction with spin. On the other hand, the only cause of spin precession and, consequently, of the spin-orbit interaction, is then the Thomas effect.<sup>5</sup> (The connection between the Thomas effect and the non-Euclidean character of velocity space is examined in Ref. 6.) When the finite size of the string is taken into account, the result is the gluomagnetic field whose amplitude is proportional to the transverse size of the string.<sup>4</sup>

The magnitude of the effect due to Thomas precession is found to be large. For  $J > 2$ , the corresponding level splitting is at first comparable with and then greater than the separation between successive orbital excitations.

We shall use the following formulas to describe experimental data that include the above effects:

$$M = \int dE + \sum_{i=1,2} E_i + \sum_{i=1,2} \vec{\omega} s_i f(E_i),$$

$$J = \int d\mathbf{j} + \sum_{i=1,2} (\mathbf{l}_i + \mathbf{s}_i).$$

These expressions give the parametric relationship between the mass  $M$  and the total angular momentum  $J$  of the string with quarks (or quark clusters) at the ends. The integrals in these formulas represent the contribution of the string,  $E_i$  are the energies of particles at the ends of the string,  $\mathbf{l}_i$  and  $\mathbf{s}_i$  are the orbital momenta and spins, respectively, and  $f(E_i)$  are functions that determine the  $ls$ -contributions to the hadron mass, which can be calculated unambiguously from string dynamics without introducing any additional parameters. The total number of parameters is minimal: they are the string tension  $\nu$  and the effective masses of particles at the ends of the string. The next step is to derive and justify theoretically these formulas. This begins with physical arguments for the idealized string model with the Thomas-type spin-orbit interaction, which can be based on the analogy between the quasiclassical derivation of the spin-orbit interaction in positronium and nonrelativistic quarkonium (small orbital excitations). The analogy is then extrapolated to relativistic quarkonium (large orbital excitations, string limit; §1). The connection between spin precession and the magnitude of the spin-orbit splitting of quantum-mechanical levels is then demonstrated by considering the example of a spin moving in a scalar potential (§2). The description of the idealized model itself is presented in §3. Experimental data and model predictions concerned with orbital excitations of multi-quark hadrons are reviewed in §4, as is the spectrum of small orbital excitations that arise from chromomagnetic effects that are also examined in §4. A brief discussion of the decay of orbitally-excited hadrons in the QCD-string model is presented in §5.

### 1. SPIN-ORBIT INTERACTION IN POSITRONIUM AND QUARKONIUM

We shall take positronium as an example of how the quasiclassical approach can be used to calculate the spin-orbit interaction energy. We shall assume that the electron and the positron revolve on circular orbits around their common center of mass with angular frequency  $\vec{\omega}$ . The electron experiences the Coulomb field of the positron, which gives it an acceleration. This in turn produces the Thomas precession of the electron spin, whose frequency is given by

$$\vec{\Omega}_T = -(\gamma - 1)\vec{\omega} \approx \frac{\alpha}{2m^2 r^3} \mathbf{l}, \quad (1.1)$$

where  $\gamma = (1 - v^2)^{-1/2}$ ,  $v$  and  $m$  are, respectively, the electron velocity and mass,  $r$  is the separation between the electron and the positron,  $\mathbf{l}$  is the orbital angular momentum of the system, and  $\alpha$  is the fine-structure constant. We know that the Thomas effect arises because the rest frame of the electron is not an inertial frame in this case. In other words, the effect is the result of the non-Euclidian character of the relative-velocity space which has the Lobachevskii metric with curvature  $K = -1$ . The Thomas precession frequency measured against a laboratory clock is uniquely determined by the velocity and acceleration of the particle:

$$\vec{\Omega}_T = -(\gamma - 1) \frac{[\dot{\mathbf{v}}]}{v^2}.$$

For circular motion, this readily leads to (1.1).

Next, the positron moving relative to the electron produces a magnetic field  $\mathbf{H}$  in the rest frame of the electron, which interacts with the spin of the electron and also gives rise to its precession. The frequency of this precession is

$$\vec{\Omega}_H = -\frac{e}{m} \mathbf{H} = \frac{2\alpha}{m^2 r^3} \mathbf{l}, \quad (1.2)$$

where  $e$  is the charge of the electron.

The total precession frequency of the electron spin,  $\vec{\Omega} = \vec{\Omega}_T + \vec{\Omega}_H$ , is therefore given by

$$\vec{\Omega} = \frac{3\alpha}{2m^2 r^3} \mathbf{l}. \quad (1.3)$$

The corresponding contribution to the energy is  $\vec{\Omega} \cdot \mathbf{s}_-$ , where  $\mathbf{s}_-$  is the spin of the electron. This is the spin-orbit part of the Breit potential of positronium associated with the electron.<sup>7</sup>

$$V_{ls} = \vec{\Omega} \cdot (\mathbf{s}_- + \mathbf{s}_+) = \frac{3\alpha}{2m^2 r^3} \mathbf{l} \cdot (\mathbf{s}_- + \mathbf{s}_+). \quad (1.4)$$

Let us now consider the quark-antiquark system. The essential difference between this and positronium is the confinement effect that we shall take into account in the spirit of the bag model.<sup>8</sup> We shall assume (and here we differ from the traditional version of the model) that quarks with effective masses  $m_q \sim 1/3$  GeV are nonrelativistic (small orbital excitation) and that the quark-confining bag is spherical.<sup>9</sup> According to the bag model, confinement then means that, first, the energy necessary to produce the bag that contains the quarks and the fields due to them is  $(4\pi/3)R^3 B$ , where  $R$  is the bag radius and  $B$  is the difference between the vacuum energy densities outside and inside the bag. Second, the gluoelectric field satisfies the condition  $\mathbf{n} \cdot \mathbf{E}^a = 0$  on the bag surface, where  $\mathbf{n}$  is the unit normal to this surface. This condition can be satisfied only if the resultant color charge of the quark and antiquark is zero, i.e., only white states are allowed. In accordance with the boundary condition for the gluoelectric field, the static solution for this field inside the bag is<sup>9</sup>

$$\mathbf{E}^a = E_{\text{Coul}}^a + E_{\text{ind}}^a,$$

$$E_{\text{Coul}}^a = g^a \left( \mathbf{r} - 3 \frac{\mathbf{x}(\mathbf{x} \cdot \mathbf{r})}{x^2} \right) x^{-3},$$

and for  $x \gg r$

$$E_{\text{ind}}^a = g^a \frac{2\mathbf{r}}{R^3}, \quad (1.5)$$

where  $g^a$  is the color charge of the quark (which includes the coupling constant),  $\mathbf{r}$  is the separation between the quarks,  $R$  is the bag radius,  $\mathbf{x}$  is the distance between the center of mass of the system and the point of observation,  $E_{\text{ind}}^a$  is the gluoelectric field which is constant inside the bag (i.e., independent of  $\mathbf{x}$ ), and the divergence of this field inside the bag is zero because it has no sources there. The specific form of  $E_{\text{ind}}^a$  is given by the boundary condition

$$\mathbf{n} \cdot (\mathbf{E}_{\text{Coul}}^a + \mathbf{E}_{\text{ind}}^a) = 0.$$

In equilibrium, in which the sum of the electrostatic and vacuum energies  $[(4\pi/3)R^3 B - (g^2/r) + (g^2 r^2/R^3)]$  is a minimum in  $R$ , we have  $R^3 \sim r$ .

It will be important for our analysis to know the source

of the field  $E_{\text{ind}}^a$  induced inside the bag. If the vacuum outside the bag is a dual superconductor,<sup>3,10</sup> the field  $E_{\text{ind}}^a$  is due to currents of colored magnetic monopoles circulating on the surface of the bag. The form of  $E_{\text{ind}}^a$  readily leads to the surface density of these currents:<sup>4</sup>

$$\mathbf{j}^a = g^a \frac{3[\mathbf{m}]}{4\pi R^3}. \quad (1.6)$$

The striking fact is that the glueelectric field outside the bag is then identically zero, as expected for the dual superconductor. Suppose now that the quark-antiquark system rotates around a common center of mass with frequency  $\omega$ . The spin of a quark must then precess with a frequency whose Thomas component is

$$\vec{\Omega}_T = -(\gamma - 1)\vec{\omega} \approx -\frac{g^2}{2m_q^2 r^3} \mathbf{1} - \frac{v_{\text{sph}}}{2m_q^2 r} \mathbf{1}, \quad (1.7)$$

where  $v_{\text{sph}} = g^a E_{\text{ind}}^a = 2g^2 r/R^3$  is the additional (as compared with the Coulomb) force acting on the quark (we note that this force is independent of distance for  $R^3 \sim r$ ). The magnetic component of the quark spin precession is coupled to the magnetic field produced in the rest frame of the quark by both the moving antiquark and the 'moving' surface currents. It is given by

$$\vec{\Omega}_H = -\frac{g^a \mathbf{H}^a}{m_q} = \frac{2g^2}{m_q^2 r^3} \mathbf{1} + \frac{v_{\text{sph}}}{5m_q^2 r} \mathbf{1}. \quad (1.8)$$

The resultant frequency  $\vec{\Omega} = \vec{\Omega}_T + \vec{\Omega}_H$  is

$$\vec{\Omega} = \frac{3g^2}{2m_q^2 r^3} \mathbf{1} - \frac{3}{10} \frac{v_{\text{sph}}}{m_q^2 r} \mathbf{1}. \quad (1.9)$$

The second term in (1.9) is the bare 'string' contribution to the quark spin precession. So far, this term has been small in comparison with the first, i.e., Coulomb, contribution (we assume that  $r \ll R$ ). The conditions  $r \ll R$  and  $r \sim R^3$  are not mutually inconsistent if  $r \ll B^{-1/4}$ , i.e., if  $r$  is much less than the characteristic hadronic scale determined by the constant  $B$ .

Let us now increase the orbital angular momentum of the system. The quark-antiquark separation will then be greater, and the bag will stretch out into a string.<sup>11</sup> We shall assume that the effect of the antiquark on the quark can be neglected, i.e., the force acting on the quark is largely due to the surface magnetic currents. We then have

$$\begin{aligned} \vec{\Omega}_T &= -(\gamma - 1)\vec{\omega}, \\ \vec{\Omega}_H &= -\frac{g^a}{\gamma m_q} \mathbf{H}^a = C \frac{\gamma v d}{m_q} \vec{\omega}; \end{aligned} \quad (1.10)$$

where we have taken into account the fact that  $H^a \sim v E^a \sim \gamma^2 \omega \hat{O} |E^a$ , since  $E^a$  and  $H^a$  are adjacent parts of the string (separated by distances of the order of the string diameter  $d$ ) and  $g^a E^a = v$  is the force acting on the quarks (string tension). The relation between  $v$  and  $v_{\text{sph}}$  is<sup>9</sup>  $v = (3/2)^{1/2} v_{\text{sph}}$ . The coefficient  $C$ , which depends on the shape of the end of the string, will not be calculated. In the limit of a thin string ( $d \rightarrow 0$ ,  $v = \text{const}$ ),  $\Omega_H \ll \Omega_T$ , so that the quark spin precession is largely due to the Thomas effect.

## 2. SPIN PRECESSION AND SPIN-ORBIT INTERACTION ENERGY

From now on we shall confine our attention to high orbital angular momenta, long strings ( $L \sim l^{1/2}$ ), and negligible Breit contributions. The string (gluon field tube) will be assumed to be thin, so that the influence of the chromomagnetic field of the string on the quark spins can be neglected and the Thomas precession is the dominant effect in spin-orbit interaction. For low velocities ( $v < 1$ ), there is no difficulty in finding the corresponding energy correction by taking the nonrelativistic Hamiltonian  $H$  so that the equation  $\dot{\mathbf{s}} = \{H, \mathbf{s}\}$  becomes the equation for spin precession  $\dot{\mathbf{s}} = \vec{\Omega}_T \cdot \mathbf{s}$ , where  $\vec{\Omega}_T$  is the Thomas frequency.<sup>12</sup> As  $l$  increases the motion of the ends of the string becomes relativistic, and  $\gamma \gg 1$ . In this region, the precession frequency  $\Omega_T$  is greater by the factor  $\gamma$  than the angular frequency  $\omega$  that characterizes the separation between neighboring rotational levels. Strictly speaking, to find the corresponding energy correction, we must then start with the relativistic quantum-mechanical equation, and solve the eigenvalue problem. However, we will proceed in a different way and examine in detail the case of a particle with spin in a scalar potential, which will produce similar spin behavior. The analogy between the two cases is that the Thomas effect is the source of spin precession in both cases. The problem of spin precession in a scalar potential can be solved exactly, and the solution gives the connection between the spin precession frequency and the spin-orbit interaction energy.

We begin by writing down the classical description of spin in a scalar potential. We then introduce quantization and use the quantum-mechanical equation (Dirac equation) to find the  $ls$ -correction to the energy. For high orbital excitations, the energy can be expressed in terms of quasiclassical variables. The results obtained for the scalar potential enable us to find the  $ls$ -splitting for a string with quarks in the case of large  $l$ , which is, of course, our main problem. In addition, the analogy with the scalar potential then enables us to include the quark spins in the action for the open Nambu string. The corresponding equation for spin precession is found to be the same as the equation for Thomas precession.

### 2.1. Particle with spin in a scalar potential

We shall use the Lagrangian formalism with constraints to describe a classical particle with spin in a scalar potential  $m = m(x)$ . A similar approach was first used by Berezin and Marinov to describe the spin of a free particle<sup>13</sup> and a particle in an electromagnetic field.<sup>14</sup> The equations describing spin precession are then found to be the same as in the classical case, which is not unexpected because they have the form  $\dot{\mathbf{s}} = \vec{\Omega} \cdot \mathbf{s}$  where Planck's constant cancels out on both sides.

In the Berezin-Marinov formalism, the particle spin is described in terms of Grassmann variables. For example, in the nonrelativistic approximation, the three-dimensional vector  $\mathbf{s}$  is written as a vector product of anticommuting Grassmann variables:

$$\mathbf{s} = \frac{1}{2} i [\xi \bar{\xi}].$$

The phase space of the particle with spin is constructed by adding a three-dimensional Grassmann space to the usual

six-dimensional space.

In the relativistic case, the spin 4-vector  $s_\mu$  is described in terms of the 4-vector  $\xi_\mu$

$$s_\mu = \frac{i}{2} \epsilon_{\mu\nu\alpha\beta} u_\nu \xi_\alpha \xi_\beta,$$

where  $u_\mu$  is the particle 4-velocity. The nonphysical longitudinal components  $\xi_\nu$  are eliminated in the Berezin–Marinov approach by introducing the additional Grassmann variable  $\xi_5$  and imposing a constraint condition. We thus postulate the following action for a free particle with spin<sup>13,14</sup>

$$S_0 = \int \{mz - \frac{i}{2} [\xi_\mu \dot{\xi}_\mu - \xi_5 \dot{\xi}_5 - (u\xi - \xi_5 \lambda)]\} d\tau;$$

where  $z = (\dot{x}^2)^{1/2}$ ,  $u_\mu = \dot{x}_\mu / z$ , and  $\lambda$  is a Lagrangian multiplier (Grassmann number).

We are interested in the motion of the particle with spin in an external scalar field which is equivalent to the introduction of a position-dependent mass  $m = m(x)$ . The action for a particle with spin in a scalar potential can be constructed to ensure a closed algebra of Poisson brackets for the Hamiltonian constraints. This is achieved by introducing a derivative interaction between the spin and the scalar field into the Lagrangian:<sup>15</sup>

$$S = S_0 + i \int (f\xi) \xi_5 z d\tau, \quad (2.1)$$

where  $f_\mu = (1/m) \partial_\mu m$ .

The spin 4-vector  $s_\mu$  is actually related only to the transverse components  $\xi_\mu$ :

$$s_\mu = \frac{i}{2} \epsilon_{\mu\nu\alpha\beta} \eta_\nu \xi_\alpha \xi_\beta, \quad \eta_\mu \eta_\nu = -i \epsilon_{\mu\nu\alpha\beta} u_\alpha s_\beta, \quad (2.2)$$

where  $\eta_\mu = \xi_\mu - u_\mu (u\xi)$ . This turns out to be important in the derivation of the precession equations containing time derivatives.

It is clear from (2.2) that  $\xi \sim \hbar^{1/2}$ . By taking the variation of the action (2.1), we obtain the equations for  $\xi$ :

$$\dot{\xi}_\mu = \frac{\lambda}{2} u_\mu + f_\mu \xi_5 z, \quad \dot{\xi}_5 = \frac{\lambda}{2} + (f\xi) z \quad (2.3)$$

with the constraint condition

$$(u\xi) - \xi_5 = 0. \quad (2.4)$$

From the equation of motion for the canonical momentum

$$p_\mu = m u_\mu + i (f\xi) \xi_5 u_\mu + \frac{i}{2} (\dot{\xi}_\mu - u_\mu (u\xi)) \frac{\lambda}{z}, \quad (2.5)$$

in which we have retained only zero-order terms in the Grassmann variables, it follows that

$$w_\mu = f_\mu - u_\mu (fu), \quad (2.6)$$

in which  $w_\mu = \dot{u}_\mu / z$ . The terms in the equation for  $\dot{p}_\mu$  that are quadratic in the Grassmann variables give higher-order corrections in  $\hbar$  to the equation of precession, but these will be of no interest to us at present.

Equations (2.3), (2.4), and (2.6) readily lead to the following equations for the transverse components:  $\dot{\eta}_\mu = -u_\mu (w\eta)z$ , and (2.2) enables us to find the analogous equation for spin precession:

$$\dot{s}_\mu = -u_\mu (ws)z. \quad (2.7)$$

This equation describes the Thomas spin precession, as expected in the absence of fields (e.g., magnetic fields) that interacts directly with the spin.

Transforming to the three-dimensional form and using  $s_0$  to denote the spin in the rest frame, we find from (2.7) that

$$\frac{ds_0}{dt} = \{\vec{\Omega}_T s_0\}, \quad \vec{\Omega}_T = -(\gamma - 1) \frac{[\mathbf{v}\dot{\mathbf{v}}]}{v^2}, \quad (2.8)$$

where  $t$  is the laboratory time. In the special case of motion on circular orbits, the Thomas precession frequency measured against a laboratory clock is  $\vec{\Omega}_T = -(\gamma - 1)\vec{\omega}$  where  $\omega$  is the rotational frequency.

The relation given by (2.4) can be rewritten in terms of the canonical momentum:

$$\Phi = p\xi - m\xi_5 = 0. \quad (2.9)$$

The Poisson brackets, defined by

$$\{A, B\}_{P.B.} = \frac{\partial A}{\partial p_\mu} \frac{\partial B}{\partial x_\mu} - \frac{\partial A}{\partial x_\mu} \frac{\partial B}{\partial p_\mu} - i \frac{\overleftarrow{A} \overrightarrow{\partial}}{\partial \xi_\mu} \frac{\overrightarrow{B}}{\partial \xi_\mu} + i \frac{\overleftarrow{A} \overrightarrow{\partial}}{\partial \xi_5} \frac{\overrightarrow{B}}{\partial \xi_5}, \quad (2.10)$$

are given by the following expression for  $A = B = \Phi$ :

$$\{\Phi, \Phi\}_{P.B.} = p^2 - m^2 - 2i(\partial_\mu m \xi_\mu) \xi_5. \quad (2.11)$$

Hence, using (2.5), we see that the algebra of Poisson brackets is closed.

We shall now attempt to calculate the spin-orbit splitting energy due to spin precession. To do this, we write the energy  $\epsilon = p_0$  in terms of the canonical variables:

$$\epsilon = [p^2 + m^2 + 2i(f\xi) \xi_5 m]^{1/2} = \epsilon_0 + i \frac{m}{\epsilon_0} (f\xi) \xi_5 \quad (2.12)$$

where  $\epsilon_0 = (p^2 + m^2)^{1/2}$ . We shall be interested in the energy correction whose sign is determined by the sign of  $\mathbf{l} \cdot \mathbf{s}_0$ . We shall consider the special case of motion on a circular orbit for which  $w_\mu = (0, \mathbf{w})$ . The sign of  $\mathbf{l} \cdot \mathbf{s}_0$  changes, for example, when we replace  $\mathbf{v}$  with  $-\mathbf{v}$ . We shall therefore separate out those terms in the energy that depend on the direction of  $\mathbf{v}$ . This will be done by writing the scalar product  $u\xi$  in the form

$$u\xi = \frac{1}{\gamma} \xi_0 - \mathbf{v} \cdot \vec{\xi}, \quad (2.13)$$

where  $\vec{\xi}$  is the Grassmann variable in the rest frame of the particle. This also means that  $s_{0i} = (i/2) \epsilon_{ikl} \xi_k \xi_l$ . From these relations we find that the spin-orbit level splitting is

$$\Delta\epsilon = \frac{m' |\mathbf{p}|}{\epsilon_0^2}, \quad (2.14)$$

where the level with positive  $\mathbf{l} \cdot \mathbf{s}_0$  has the lower energy. If we use the classical equation of motion, we can rewrite this correction in the form  $\Delta\epsilon = \gamma\omega$ . In the relativistic region, the spin-orbit splitting that we have obtained is the same as the exact energy corresponding to the Thomas precession, i.e.,  $\Delta\epsilon_T = (\gamma - 1)\omega$ . The term with  $-1$  can be obtained by considering the quantum-mechanical equation with allowance for the dependence of the states themselves on  $\mathbf{l} \cdot \mathbf{s}$ .

As for the free particle with spin, quantization involves the replacement of  $\xi$  with the operators

$$\hat{\xi}_\mu = \left(\frac{\hbar}{2}\right)^{1/2} \gamma_5 \gamma_\mu, \quad \hat{\xi}_5 = \left(\frac{\hbar}{2}\right)^{1/2} \gamma_5. \quad (2.15)$$

The odd constraint (2.9) then becomes the Dirac equation

in the scalar field. The even constraint, on which the Poisson bracket (2.11) for odd coupling vanishes, becomes the corresponding integrable equation.

We also note that the external scalar field preserves the invariance under transformations associated with the freedom to choose the parameter  $\tau$ , and also invariance under the transformations

$$\begin{aligned} \xi_\mu &\rightarrow \xi_\mu + p_\mu \rho, & \xi_5 &\rightarrow \xi_5 + m\rho, \\ x_\mu &\rightarrow x_\mu + i\xi_\mu \rho, \end{aligned} \quad (2.16)$$

which constitute the simplest example of supersymmetric transformations.

## 2.2. The $ls$ -coupling energy in a scalar potential

We shall now calculate the spin-precession energy, taking the quantum-mechanical equations<sup>16</sup> as our starting point. In contrast to the standard procedure for taking  $ls$ -coupling into account, which involves an expansion in powers of  $v/c$ , the method presented below is valid in the general case, including the ultrarelativistic limit.

The solution of the Dirac equation  $(\hat{p} - m)\psi = 0$  for a scalar potential  $m = m(r)$  can be written in the form

$$\psi = \begin{pmatrix} f(r)\Omega_{jlm} \\ (-1)^{(l+l')/2}g(r)\Omega_{j'l'm} \end{pmatrix}, \quad l + l' = 2j \quad (2.17)$$

where we are using the notation adopted in Ref. 7 in which  $j$  is the total angular momentum. The functions  $f$  and  $g$  satisfy the following set of differential equations:

$$\begin{aligned} (fr)' + \kappa f - (\varepsilon + m)gr &= 0, \\ (gr)' - \kappa g + (\varepsilon - m)fr &= 0, \end{aligned} \quad (2.18)$$

where  $\kappa = -(1 + l\partial)$ . This set of equations is readily reduced to the second-order equation for the function  $F = fr/(\varepsilon + m)^{1/2}$

$$F'' + (\varepsilon^2 - V^2(\varepsilon, r))F = 0, \quad (2.19)$$

where

$$V^2(\varepsilon, r) = \frac{l(l+1)}{r^2} + m^2 + \frac{3}{4} \left( \frac{m'}{\varepsilon + m} \right)^2 - \frac{1}{2} \frac{m''}{\varepsilon + m} + \frac{\kappa}{r} \frac{m'}{\varepsilon + m}. \quad (2.20)$$

We shall be interested in positive values of  $\varepsilon$  for which (2.19) has solutions that vanish at  $r = 0$  and  $\infty$ . For potentials of the form  $m \sim r^n$  and  $l \gg n$ , the last three terms in  $V^2$  can be treated as a perturbation. Near the minimum ( $r = r_0$ ) of the function  $l(l+1)/r^2 + m^2$ , we can use the approximate expression

$$\begin{aligned} \tilde{V}^2 &= V^2(\varepsilon_0, r_0) + k^4(r - r_0)^2, & \varepsilon_0 &= \left[ \frac{l(l+1)}{r_0^2} + m^2(r_0) \right]^{1/2}, \\ k^4 &= \frac{1}{2} \left[ \frac{l(l+1)}{r^2} + m^2 \right]'' \Big|_{r=r_0}. \end{aligned} \quad (2.21)$$

Hence, for large  $l$ , the motion is quasiclassical and the lowest eigenvalue  $\varepsilon^2$  can be calculated from the formula

$$\varepsilon^2 = V^2(\varepsilon_0, r_0) + k^2. \quad (2.22)$$

By definition of  $r_0$ , we have

$$m'(r_0) = (\varepsilon_0^2 - m^2(r_0))/r_0 m(r_0). \quad (2.23)$$

The  $ls$ -correction to the energy can now be found from (2.20):

$$\Delta\varepsilon_\kappa = (\gamma - 1) \frac{\kappa}{2r_0^2 \varepsilon_0}, \quad \gamma = \frac{\varepsilon_0}{m(r_0)}. \quad (2.24)$$

Hence the separation between levels with opposite spin orientations relative to  $l$  is

$$\Delta\varepsilon_{ls} = (\gamma - 1)\omega, \quad (2.25)$$

where  $\omega$  is the separation between neighboring rotational levels with the same sign of  $l$ 's. For a potential that increases in accordance with a power-type law, we have  $\gamma = (n + 1)^{1/2}$ . The quantity  $k \sim l^{1/2} n^{1/4}/r_0$  then characterizes the radial momentum, and (2.24)–(2.25) are valid when  $K \ll m(r_0) \sim 1/r_0 n^{1/2}$ .

For an exponentially growing potential  $m = \mu \exp(\alpha r)$ , the most interesting region corresponds to orbital momenta for which

$$\frac{\mu}{\alpha} e^{\alpha r_0} > 1, \quad (2.26)$$

where  $r_0$  is a solution of

$$\alpha r_0 = \left( \frac{\alpha l}{\mu} e^{\alpha r_0} \right)^{2/3} \quad (2.27)$$

It can be shown that rotation can be relativistic only when (2.26) is satisfied. As before, the effective mass is determined by the quantity  $m(r_0)$ . We have  $\gamma \sim (\alpha r_0)^{1/2}$  from which it is clear that the motion becomes relativistic for  $l \gg \mu/\alpha$ . If, however,  $\mu/\alpha \ll 1$ , but  $l \gg \mu/\alpha$ , we have  $(\mu/\alpha) \exp(\alpha r_0) \gg 1$  and the  $\gamma$ -factor lies in the range  $[\ln(\alpha/\mu)]^{1/2} \ll \gamma \ll l^{1/3}$ .

Condition (2.26) is automatically satisfied if  $\mu/\alpha \gg 1$ , in which case  $1 \ll \gamma \ll l^{1/3}$ .

We note that for all the above potentials there is a region for which  $k \gg m(r_0)$ . For example, for the exponentially growing potential, the condition  $k \gg m(r_0)$  is satisfied for  $l^{2/3} \ll \ln(\alpha/\mu)$ . However, in this case, the  $\gamma$ -factor, which is now characterized by the ratio  $\varepsilon_0/k$ , satisfies the condition  $v\gamma \ll l^{-1/6}$ , i.e., the motion is nonrelativistic.

It is clear from these examples that the situation in which the effective fermion mass is due to the radial localization of the fermion, and is determined by  $k$ , while the motion in the quasiclassical region is relativistic, can occur in potentials that increase more rapidly than the exponential potential. An example of this is provided by a fermion in a spherical cavity of fixed radius  $R$ . The condition on the boundary, which ensures that the particle remains confined, and is consistent with the Dirac equation, is<sup>8</sup>

$$i n_\mu \gamma_\mu \psi = \psi. \quad (2.28)$$

This condition violates the  $\gamma_5$  invariance, as indeed should be the case in scalar confinement. The fermion is initially assumed to be massless, so that the function  $\psi$  satisfies the free Dirac equation  $\hat{p}\psi = 0$  inside the cavity. The problem can be solved exactly (see Appendix 1), and the resulting value of the spin-orbit splitting energy is, as before, greater by a factor of  $\gamma$  than the separation between neighboring rotational states.

It will be useful later to have one other way of calculat-

ing the  $ls$ -splitting energy in a scalar potential. Let us evaluate the expectation value of the square of the Hamiltonian:  $\langle H^2 \rangle = \int \psi^\dagger H^2 \psi, d^3r$ . For a Dirac particle,  $H = \vec{\alpha} \cdot \mathbf{p} + \beta m$ , so that

$$H^2 = \mathbf{p}^2 + m^2 + im'(\mathbf{n}\vec{\sigma}). \quad (2.29)$$

The result for  $\Delta \varepsilon_{ls}$  (Appendix 2) is identical with (2.25), and the contribution proportional to  $\gamma$  arises from the term containing  $m'$  whereas the  $-1$  term occurs when the  $\mathbf{l} \cdot \mathbf{s}$  dependence of the wave function is taken into account.

It is now convenient to recall the attempt to perform a classical calculation of the energy correction (see last Section). The spin-dependent correction to  $\varepsilon^2$  has the form  $2i(f\xi)\xi_5 m$  [see (2.12)] where  $f_\mu = (1/m)\partial_\mu m$ , so that when  $m = m(|r|)$  we have  $f_\mu = (1/m)(0, m'\mathbf{n})$ . The quantity  $2i(f\xi)\xi_5 m$  becomes  $im'(\mathbf{n}\vec{\sigma})$  in the course of quantization, which is identical with the last term in (2.29). Hence it is clear that the evaluation of the  $ls$ -splitting energy in the classical approach produces the term  $\gamma\omega$  which is the leading term in the relativistic limit. The  $-1$  term arises only in the quantum-mechanical approach in which the  $ls$  dependence of the states themselves is taken into account.

In the case of motion in a vector potential, terms proportional to  $\gamma$  in the spin precession frequency are found to cancel out. Similar cancellation occurs in the energy as well. Hence, the  $ls$ -splitting cannot be calculated for the vector potential at the classical level.

We thus arrive at the conclusion that, when the only source of spin precession is the Thomas effect, the spin-orbit splitting energy is equal to the precession frequency

$$\vec{\Omega}_T = (\gamma - 1)\vec{\omega}, \quad (2.30)$$

where the energetically most favorable orientation of the spin is along the axis of rotation. The important conclusion that follows from this is that, in the ultrarelativistic limit, the  $ls$ -splitting exceeds by a factor of exactly  $\gamma$  the separation between rotational levels and, in this sense, constitutes a significant effect.

We now turn to the formulas that will be used to calculate the mass spectra of high-spin hadrons. We begin by summarizing the conclusions of §§1 and 2. In §1, we started with positronium and calculated the spin-orbit part of the Breit potential. We then considered the  $q\bar{q}$  system and examined spin-orbit effects for small orbital excitations for which the shape of the object is still nearly spherical and the quark velocity low. We showed that there were additional contributions to the  $ls$ -coupling that were due to confinement in the  $q\bar{q}$  system. As  $l$  increases, and the hadron stretches out into a tube of chromoelectric lines of force, these contributions alter the nature of the  $ls$ -coupling both qualitatively and quantitatively, and the Thomas component of the quark spin precession begins to dominate. We shall therefore assume in our discussion below that the precession of the spins of the quarks at the ends of the relativistic string is entirely due to the Thomas effect.

In §2 we examined the connection between the quark spin precession frequency and the spin-orbit coupling energy by considering the example of a quark in a scalar potential in which the Thomas effect was the sole cause of spin. The conclusion was that the spin-orbit splitting energy was equal to the Thomas precession frequency. We shall use this result

when we consider the idealized QCD-string model in connection with the spectra of high-spin hadrons.

### 3. THE SPECTRUM OF HIGH-SPIN HADRONS IN THE MODEL OF A STRING WITH $ls$ -COUPLING

The results obtained in the preceding Sections enable us to find the connection between the total angular momentum  $J$  and the mass  $M$  (Regge trajectories) in the string model by expressing  $J$  and  $M$  in terms of the angular velocity  $\omega$  of the string. We recall that we are interested in relatively high orbital momenta for which the quasiclassical approach is valid.

The string tension  $\nu$  and the quark mass  $m_q$  will be regarded as parameters. The mass  $m_q$  will be understood to mean the effective mass of the quark, defined in the comoving frame. The reasons for the appearance of the effective mass are relatively clear. They are: the localization of the quark in the longitudinal (along the string) direction, due to the centrifugal barrier, and also localization in the transverse direction, determined by the transverse size of the string. The effective mass interpreted in this way is obviously independent of the rotational frequency of the string, so that the latter can be looked upon as a parameter.

In the quasiclassical limit, the energy (mass)  $M$  and the total angular momentum (spin)  $J$  of the string with quarks at the ends can be found from the following formulas:<sup>12,17</sup>

$$\begin{aligned} M &= \int_{-L/2}^{L/2} \frac{\nu dx}{[1 - (\omega x)^2]^{1/2}} + \frac{2m_q}{(1 - v^2)^{1/2}} + \Delta E_{ls}, \\ J &= \int_{-L/2}^{L/2} \frac{\nu \vec{\omega} x^2 dx}{[1 - (\omega x)^2]^{1/2}} + s_1 + s_2; \end{aligned} \quad (3.1)$$

where  $L$  is the length of the string and  $v = \omega L/2$  is the quark velocity. There is also an additional condition that follows from the requirement that the quark at the end of a string must be in equilibrium:

$$\frac{d|\mathbf{p}|}{d\tau} = \nu, \quad (3.2)$$

where  $\mathbf{p}$  is the quark momentum and  $\tau$  is the time measured in the comoving frame. In the laboratory frame, this condition assumes the form

$$\frac{d|\mathbf{p}|}{dt} = \nu(1 - v^2)^{1/2}, \quad (3.3)$$

which is equivalent to

$$m\nu\omega\gamma = \nu/\gamma, \quad \gamma = 1/(1 - v^2)^{1/2}. \quad (3.4)$$

Having evaluated the integrals in (3.1), and having substituted the explicit expression for the  $ls$ -coupling energy, we obtain the final result in the form

$$\begin{aligned} M &= \frac{2\nu}{\omega} \left( \arcsin v + \frac{1}{v\gamma} \right) - \vec{\omega}(s_1 + s_2)(\gamma - 1), \\ J &= s_{1\omega} + s_{2\omega} + \frac{\nu}{\omega^2} \left( \arcsin v + \frac{v}{\gamma} \right); \end{aligned} \quad (3.5)$$

where  $s_{1\omega}, s_{2\omega}$  are the projections of the quark spins onto the axis of rotation.

As the orbital angular momentum increases, the motion of the ends of the string becomes relativistic, but the relativistic regime develops relatively slowly:

$$\gamma \approx \left( \frac{2\nu}{\pi m_q^2} \right)^{1/4} l^{1/4}. \quad (3.6)$$

In this limit, the connection between the mass  $M$  and the total angular momentum  $J$  is given by

$$M^2 \approx 2\pi\nu \left\{ J + \left[ \frac{8}{3\pi} \left( \frac{\pi m_q^2}{2\nu} \right)^{3/4} - (s_1\omega + s_2\omega) \left( \frac{2\nu}{\pi m_q^2} \right)^{1/4} \right] J^{1/4} \right\}. \quad (3.7)$$

It is interesting to note that the  $ls$ -correction to the mass produces the same deviation from the linearity of the trajectory as the inclusion of nonzero quark mass in string dynamics.

An attempt to find the  $ls$ -correction to the energy of a massive fermion localized at the end of the string was also undertaken in Ref. 18, using the approach proposed in Ref. 19. The correction found in Ref. 18 in the nonrelativistic limit is identical with the correction due to the Thomas spin precession. At the same time, the spin precession equation, which is readily obtained from the equation for  $\psi$  given in Ref. 18, has nothing in common with the Thomas precession. Hence, it follows that the approach employed in Ref. 18 is not internally consistent.

The influence of spin degrees of freedom was discussed in Ref. 20 in the context of longitudinal vibrations, but no specific results were obtained for the string spectrum with allowance for quark spins.

Spin effects in orbitally excited mesons were also discussed in Ref. 21. A closed set of Hamiltonian constraints was sought for a rectilinear string with massless quarks,<sup>21,22</sup> whose spins were described in terms of the Grassmann variables. Four Regge trajectories corresponding to different orientations of quark spins were obtained after quantization of this degenerate system by the Dirac method. Experimental data on meson trajectories were described in terms of four adjustable parameters, fitted to each quartet of trajectories, and the common slope  $\alpha'$ . The spin-orbit splittings were found in this model to be small and practically constant for large  $J$ , and  $M_{j=l+1}^2 \ll M_{j=l}^2 \ll M_{j=l-1}^2$ . We shall see that the explicit inclusion of Thomas precession leads to significantly different predictions: the spin-orbit splitting is found to be comparable with the separation between neighboring resonances on a given trajectory, and the ordering of the levels is such that states with maximum total spin have lower energy for given  $l$ .

#### 4. DESCRIPTION OF EXPERIMENTAL DATA

The formulas given by (3.1)–(3.5), which determine the relationships between  $J$  and  $M$ , can be generalized in a fairly obvious way to the case of different quark or quark cluster masses at the ends of the string:

$$M = \frac{\nu}{\omega} \left( \arcsin v_1 + \arcsin v_2 + \frac{1}{v_1\gamma_1} + \frac{1}{v_2\gamma_2} \right) - s_1\omega(\gamma_1 - 1) - s_2\omega(\gamma_2 - 1), \quad (4.1)$$

$$J = s_1 + s_2 + \frac{\nu}{2\omega^2} \left( \arcsin v_1 + \arcsin v_2 + \frac{v_1}{\gamma_1} + \frac{v_2}{\gamma_2} \right), \quad (4.2)$$

and the conditions for the equilibrium of the quarks at the ends of the string are

$$\omega\mu_1 v_1 \gamma_1^2 = \nu, \quad \omega\mu_2 v_2 \gamma_2^2 = \nu; \quad (4.3)$$

where  $\mu_1, \mu_2$  are the quark masses,  $v_1, v_2$  are the quark velocities, and  $\gamma_i = (1 - v_i^2)^{-1/2}$ . When  $\mu_1 \neq \mu_2$ , there are additional conditions that determine the position of the center of gravity of the string with quarks:

$$\omega x_1 = \nu, \quad \omega x_2 = \nu. \quad (4.4)$$

It is readily verified that the momentum of a string segment  $x_1$  with cluster  $\mu_1$  is equal to minus the momentum of a segment  $x_2$  of a string with cluster  $\mu_2$ . For given  $\mu_1, \mu_2$ , and  $\nu$ , the formulas given by (4.1)–(4.3) give the dependence of  $J$  on  $M$  in parametric form.

We begin our description of experimental data by considering orbitally excited mesons  $q\bar{q}$  ( $q = u$  or  $d$ ) with quantum numbers  $J^{PC} = 1^{--}, 2^{++}, 3^{--}, \dots$  ( $\rho, \omega$  trajectories).<sup>23</sup> The position of the particles on the  $(M^2, J)$  plot is defined by (4.1)–(4.3) with

$$\mu_1 = \mu_2 = m_q, \quad s_1 = s_2 = 1/2.$$

The parameters  $m_q$  and  $\nu$  are determined by the masses of the two particles with the appropriate quantum numbers. We recall that the model must work for high orbital excitations, so that it is more correct to choose high-spin particles when the parameters are determined. Since there is no isospin dependence in (4.1)–(4.3), the model predicts degeneracy in total isospin (in this case  $T = 0$  or  $1$ ). If we take  $m_q$  and  $\nu$  in accordance with (4.1)–(4.3), we can uniquely predict the positions of the remaining particles on the  $\omega$  and  $\rho$  trajectories, and also the masses of orbitally excited analogs of pions with quantum numbers  $J^{PC} = 1^{+-}, 2^{-+}, 3^{+-}, \dots$  that are degenerate in terms of mass with particles with  $T = 0$ .

The next step is to determine the masses of orbitally excited strange mesons  $q\bar{s}$ . This can be done by introducing only one additional parameter, namely, the effective mass  $m_s$  of the strange quark, which can be determined from the position of a single point, say, a point on the  $K^*$  trajectory. The remaining masses of the  $q\bar{s}$  levels, and also the masses of mesons  $s\bar{s}$  with hidden strangeness, are predicted unambiguously. Similarly, the behavior of the mass of the charmed quark  $m_c$  enables us to calculate the mass of the orbitally excited analogues  $D, D^+, D_s, \text{ and } D_s^*$  of the  $\eta_c$  and  $\psi$  mesons. Mesons consisting of a light and a heavy quark occupy a special place and will be discussed in a separate Section.

To calculate the masses of orbitally excited strange baryons, we have to introduce two new parameters, namely the masses of the strange diquarks  $qq$  where  $T = S = 0$  or  $1$  (denoted by  $m_0$  and  $m_1$ , respectively). We shall see that of all the possible configurations describing orbital excitations of baryons, the energetically most convenient is the configuration consisting of a quark and a diquark at different ends of the string. In general terms, this is the scheme that we shall use to calculate the masses of orbitally excited hadrons, and then compare the predictions of the model with experiment.

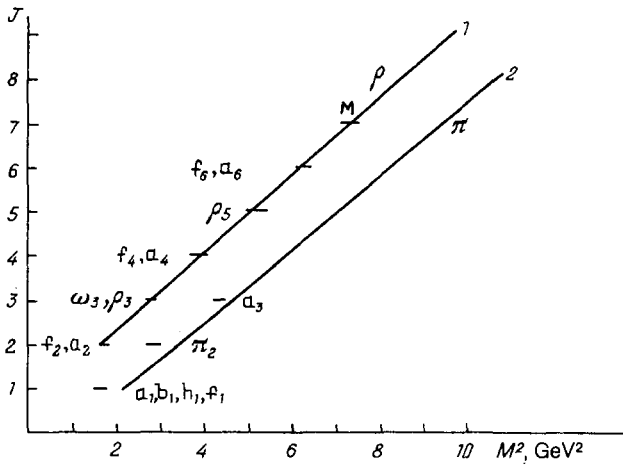


FIG. 1. Masses of orbitally excited  $q\bar{q}$  ( $q = u, d$ ).

Our calculations will be presented in the form of trajectories on the  $(M^2, J)$  plot; the experimental data will be taken from the tables reproduced in Ref. 1.

#### 4.1. $q\bar{q}$ mesons ( $q = u, d$ )

The string tension  $\nu$  and the effective mass  $m_q$  of the light quark, which are involved in calculations of the mass of the  $q\bar{q}$  states and are fixed as indicated above, are as follows:

$$m_q = 340 \text{ MeV}, \quad (2\pi\nu)^{1/2} = 1,07 \text{ GeV}.$$

In Fig. 1, trajectory 1 (the  $\rho$  trajectory) corresponds to quark spins aligned along 1. The quantum numbers of the particles on this trajectory are  $J^{PC} = 2^{++}, 3^{--}, \dots$  and  $T = 0$  or 1. Experimental data are in good agreement with the predictions of this model. Trajectory 2 has a different projection of the spin of one of the quarks ( $s_1 = -s_2 = +1/2$ ). The Thomas correction is zero in this case. The quantum numbers of particles on this trajectory are  $J^{PC} = 1^{+-}, 2^{-+}, 3^{+-}, \dots, T = 0$  or 1 ( $\pi$  trajectory). The number of states on trajectory 2 is greater by a factor of 2 because the quark spins can add to 0 or 1.

The mutual disposition of the particles on trajectories 1 and 2 is in fact determined by the spin-orbit splitting: the model predicts that a particle with spin  $J$  and parity  $P$  on trajectory 1 should be lighter (by the amount corresponding to the Thomas shift) than the particle with spin  $J - 1$  and the same parity  $P$  on trajectory 2. Experimental data obtained for low  $J$  are in conflict with this prediction (the case of low  $J$  will be discussed below in greater detail). However, when  $l = 3$  ( $J = 3$  on trajectory 2), there are indications of qualitative agreement. Unfortunately, there is a lack of experimental data for higher spins on trajectory 2, and it is precisely this region that is of particular interest from the point of view of spin-orbit effects predicted by the string model.

#### 4.2. $q\bar{s}$ and $s\bar{s}$ mesons

The introduction of only one further parameter, namely, the mass of the strange quark, enables us to calculate the spectrum of orbital excitations of  $K$ ,  $K^*$ , and  $\varphi$  mesons. These predictions are again deduced from (4.1)–(4.3). The mass of the strange quark can be determined, for example, from the mass of  $K^*(1780)$  with  $J^P = 3^-$ . This gives

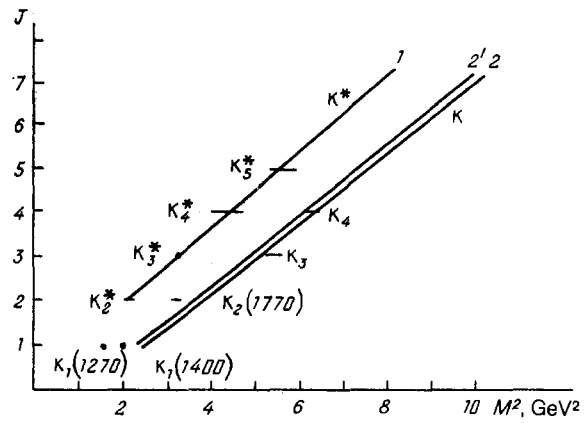


FIG. 2. Masses of orbitally excited strange mesons.

$m_s = 440 \text{ MeV}$ . The predicted masses of the remaining orbital excitations of  $K^*$  mesons are indicated by trajectory 1 in Fig. 2. The spins of both quarks are aligned along the axis of rotation in such a way that the total angular momentum  $J$  is a maximum for given orbital angular momentum. If we know the quark masses we can also calculate the spectrum of orbital excitations of  $K$ -mesons with quantum numbers  $J^P = 1^+, 2^-, 3^+$ , and so on. The model predictions are shown by trajectories 2 and 2' in Fig. 2. The sum of the projections of quark spins is then zero, and  $J = l$ . The resultant spin of the quarks can be 0 or 1, so that the number of states is greater by a factor of 2. Trajectories 2 and 2' correspond to different superpositions of states with different total quark spins.

Figure 2 also shows the experimentally established particles. The absence from the kaon spectrum of lighter particles with quantum numbers  $J^P = 3^+$  and  $4^-$  could be a serious argument in support of the hypothesis that the spin-orbit interaction is due to the Thomas precession.

If we know the string tension and the effective mass of the strange quark, we can calculate the mass spectrum of the orbitally excited analogs of the  $\varphi$ -meson with  $J^{PC} = 2^{++}, 3^{--}, 4^{++}$ , and so on. The model predictions are shown in Fig. 3 (trajectory 3) and are compared with experimental data. Figure 3 also shows the predicted mass spectrum of the orbitally excited system  $s\bar{s}$  with quantum numbers  $J^{PC} = 1^{+-}, 2^{-+}, 3^{+-}$ , and so on. The trajectories shown in Figures 2–3 exhaust the predictions of the model

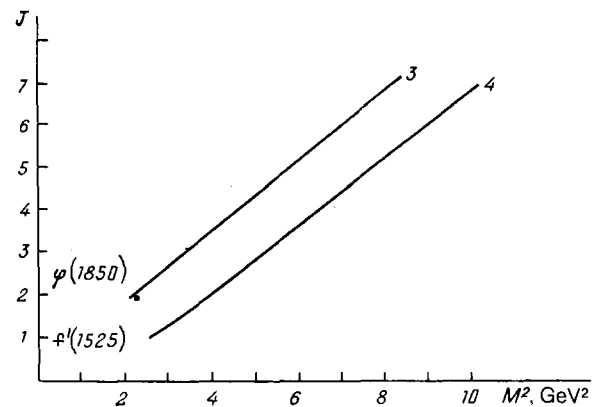


FIG. 3. Masses of orbitally excited  $s\bar{s}$ .

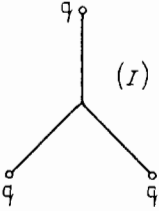


FIG. 4.

for the mass spectrum of the lightest excited states of  $q\bar{s}$  and  $s\bar{s}$  with all the possible quantum numbers  $J^P$ . The ground states of  $K$  and  $K^*$  do not, of course, appear in this discussion.

#### 4.3. Orbital excitations of baryons

A number of additional questions arises when the mass spectrum of orbitally excited baryons is calculated. The first is: what is the configuration that corresponds to the minimum mass of a state for given quantum numbers? We can imagine three different possible configurations describing orbital excitations of baryons (Figs. 4–6). (In all three cases, the string tension is, of course, the same as for the mesons and is equal to  $\nu$ .) Let us compare the energies corresponding to these configurations, assuming that the quark spins are aligned along the axis of rotation. We can then readily see that the configuration indicated by the star in Fig. 4 corresponds to the following dependence of  $M$  on  $J$  (as before, defined parametrically):

$$M_I = \frac{3}{2}M, \quad J_I = \frac{3}{2}J, \quad (4.5)$$

where  $M$  and  $J$  are given by (4.1)–(4.3) with  $\mu_1 = \mu_2 = m_q$ . For large  $J$ ,

$$M_I^2 = \frac{3}{2}(2\pi\nu)J_I. \quad (4.6)$$

The energy corresponding to the configurations of Fig. 5 can also be readily calculated from the formulas that specify the meson trajectory:

$$M_{II} = M + m_q, \quad J_{II} = J + \frac{1}{2}. \quad (4.7)$$

However, it is clear that this configuration is unstable because the centrifugal force (in the absence of the spin-spin interaction) tends to push the quark toward the end of the string. We shall not examine this configuration any further.

The energy of the configuration shown in Fig. 6 depends on the mass of the diquark. For high angular momenta, when the contribution of the diquark mass can be neglected, we have

$$M_{III}^2 = 2\pi\nu J_{III}. \quad (4.8)$$

Comparison of (4.6) and (4.8) shows that the star-type configuration is energetically inconvenient at high  $J$ . Finally, for low  $J$  (orbital angular momentum  $\geq 1$ ) we must take into

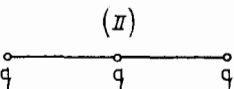


FIG. 5.

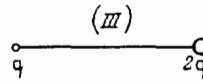


FIG. 6.

account all the terms in  $M$  and  $J$ . The choice of the most energetically convenient configuration can then be solved only numerically. Anticipating a little, we note that, for low  $J$ , the most convenient configuration is the one with a quark at one end and a diquark at the other.<sup>23,24</sup> The mass of the diquark must be known before we can calculate the energy and the angular momentum. We note that, in this situation, the very concept of the mass of a colored cluster is meaningful if the localization of the quarks along the string by the centrifugal force does not change with increasing  $J$ . If we use the arguments put forward in Ref. 4, we can show that the localization of the quark in the longitudinal direction is of the order of  $\Delta L = L/J^{1/2}$  where  $L$  is the string length. For high angular momenta,  $L \approx 4J^{1/2}/(2\pi\nu)^{1/2}$ , so that  $\Delta L \sim 4/(2\pi\nu)^{1/2}$ . The localization of the quark in the transverse direction will obviously not change either because it is determined by the cross section of the string, and the string properties do not depend on  $J$ . The diquarks in baryons are antisymmetric in color, so that  $T = S = 0$  or 1.

We begin with states that have the maximum possible spins, taking first the lowest orbital excitations ( $l = 1$ ). Then, by identifying the predicted particles with experimental data, we attempt to determine the diquark masses.

It is clear that baryons with a triplet diquark should have the lowest mass for given spin  $J$ . Particles with quantum numbers  $J^P = 5/2^-, 7/2^+, 9/2^-,$  and so on should lie on this trajectory. This prediction is in agreement with experiment. As in the case of mesons, the model predicts degeneracy in isospin. Since the diquark isospin is 1, baryons with  $T_B = 1/2(N)$  and  $T_B = 3/2(\Delta)$  should lie on this trajectory. The trajectory is defined by (4.1)–(4.3) with

$$\mu_1 = m_q, \quad s_1 = 1/2; \quad \mu_2 = m_1, \quad s_2 = 1.$$

Figure 7 shows the predictions of our model, i.e., the trajectory  $(N - \Delta)_1$  for  $m_1 = 550$  MeV. It also shows the experimentally identified particles with the lowest masses for the corresponding quantum numbers  $J^P$ . Judging by this

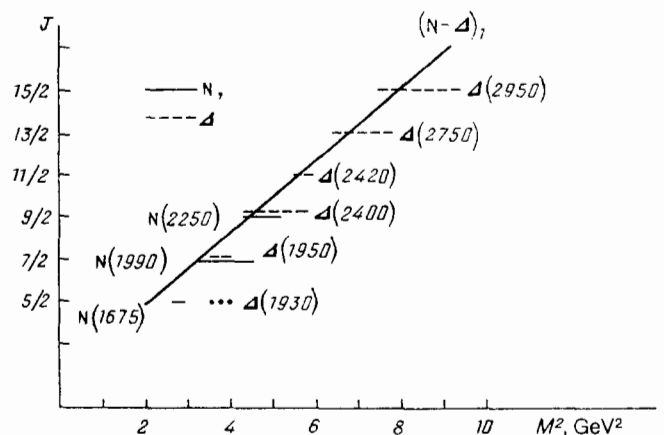


FIG. 7. Masses of orbitally excited levels of the system  $q - qq_1$  with  $J^P = 5/2^-, 7/2^+, \dots, T = 1/2, 3/2$ .

figure, the model agrees with the experiment, beginning with  $J = 7/2$  (which corresponds to  $l = 2$ ) onward. The discrepancy between the model predictions and experimental data for small  $J$  suggests that the chromomagnetic field must be taken into account. This is discussed in some detail later. Clearly, these effects are important only for the lowest orbital excitations. It is also important to recall that, strictly speaking, the model is not valid for the lowest orbital excitations, so that we can conclude that there is qualitative agreement with experiment for low  $J$ . Usually, the  $T_B = 3/2$  baryons shown in Fig. 7 describe the so-called  $\Delta$  trajectory (see, for example, Ref. 25). The isospin degeneracy predicted by the string model appears to agree with experiment (see Fig. 7). It would be interesting to verify this prediction for higher spins.

Let us now consider trajectories with a singlet diquark, for which the spin of the quark sitting at one end of the string and the orbital angular momentum combine so as to produce the highest possible result. The lightest baryons with  $J^P = 3/2^-, 5/2^+, 7/2^-,$  and so on should lie on this trajectory. The diquark isospin is zero, so that the total isospin is fixed at  $T_B = 1/2$ . Experimentally identified baryons that satisfy these criteria are usually described by a nucleon trajectory ( $N_\alpha$  trajectory<sup>25</sup>). The number of such particles is small: apart from the proton (which does not fit our diquark classification of trajectories), only two nucleon resonances have been established experimentally, namely,  $N(1680)$  with  $J^P = 5/2^+$  and  $N(2220)$  with  $J^P = 9/2^+$ . We note that the mass of  $N(1680)$  is practically the same as the mass of  $\omega_3(3^-)$ . Both these particles are described in the string model as orbital excitations with  $l = 2$ , and one of them is obtained from the other by replacing the antiquark with the singlet diquark. Since the spin-orbit correction for mesons is roughly speaking twice as high, the singlet diquark is lighter than the quark, and is substantially lighter than the triplet diquark. A numerical fit carried out for the mass of the  $N(1680)$  gives  $m_0 = 220$  MeV. We note that  $m_1 - m_0 \approx (m_p - m_\pi)/2$ . This would be the case if the spin mass splittings were determined in both situations by the interaction between the colored magnetic moments of the quark.

The model predictions for other nucleon excitations involving the singlet diquark are shown in Fig. 8 ( $N_1$  trajectory). This was calculated from (4.1)–(4.3) with

$$\mu_1 = m_q, \quad s_1 = 1/2; \quad \mu_2 = m_0, \quad s_2 = 0.$$

The experimental data of Fig. 8 include the baryon with  $J^P = 13/2^+$ . In the 1990 tables of elementary particles,<sup>1</sup> this particle is shown as  $N(2700)$ . Two experiments are cited in support of this, but their results do not overlap. They are  $3000 \pm 100$  and  $2612 \pm 45$  MeV. It is possible that these results are more correctly interpreted as providing evidence for the existence of two nucleon resonances. One of them (with the lower mass) is shown in Fig. 8 and the other will be taken into account below<sup>1)</sup>. Figure 8 also shows the data for  $N(1520)$  and  $N(1700)$  with quantum numbers  $J^P = 3/2^-$ , which can be interpreted as the first orbital excitation of the nucleon. There is, of course, little hope of quantitative agreement. In addition to magnetic effects, we must also take into account configuration mixing. We note that the ground state of the nucleon has an equal probability of containing diquarks with  $S = 1$  or  $S = 0$ . Appreciable mixing of configu-

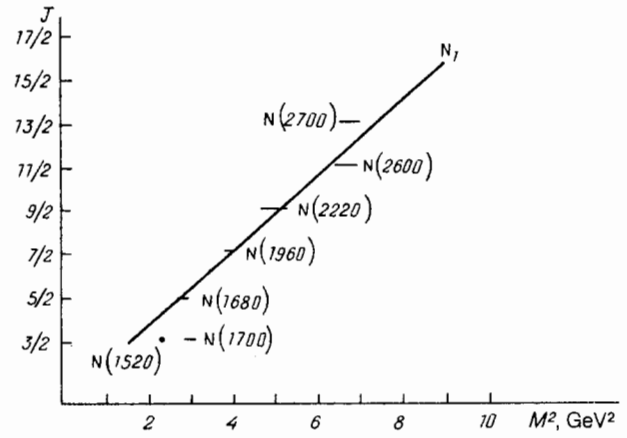


FIG. 8. Masses of orbitally excited baryons  $q - qq_0$  with  $J^P = 3/2^-, 5/2^+, \dots, T = 1/2$ .

rations with different diquark spins can also occur for the lower orbital excitations. In this sense, baryons with  $J^P = 3/2^-$  are superpositions of states lying on different trajectories. We note that the concept of clusterization is valid for small configuration mixing. Judging by Fig. 8, configuration mixing and chromomagnetic field effects become relatively insignificant from  $l = 2$  onward (on the  $N_1$  trajectory this corresponds to  $J^P = 5/2^+$ ).

#### 4.4. Other baryon trajectories

So far, we have confined our attention to baryon excitations in which the particle spins at the ends of the string have the most favorable orientations for spin-orbit coupling. We now consider states with the triplet diquark for which  $J = l + 1/2$ . As on the  $(N - \Delta)_1$  trajectory, here again we should have isospin degeneracy. Moreover, the resultant quark spin should be  $1/2$  or  $3/2$ , so that the number of  $N$  and  $\Delta$  states is greater by a factor of 2. In the string model,  $J = l + 1/2$  can occur in two different ways:

$$s_1 = \frac{1}{2}, \quad s_2 = 0,$$

$$s_1 = -\frac{1}{2}, \quad s_2 = 1$$

(we recall that the diquark mass  $m_1$  is already fixed). The corresponding trajectories will be denoted by  $(N - \Delta)_2$  and  $(N - \Delta)_2'$  (Fig. 9). Particles with  $J^P = 3/2^-, 5/2^+, 7/2^-$ , and so on lie on these trajectories. The trajectories  $(N - \Delta)_2$  and  $(N - \Delta)_2'$  correspond to the different superpositions of states with different resultant quark spins

$$\psi = \left(\frac{2}{3}\right)^{1/2} \psi\left(\frac{3}{2}, +\frac{1}{2}\right) - \left(\frac{1}{3}\right)^{1/2} \psi\left(\frac{1}{2}, +\frac{1}{2}\right), \quad (4.9)$$

$$\psi' = \left(\frac{1}{3}\right)^{1/2} \psi\left(\frac{3}{2}, +\frac{1}{2}\right) + \left(\frac{2}{3}\right)^{1/2} \psi\left(\frac{1}{2}, +\frac{1}{2}\right).$$

Of course, in reality, the superposition of states must be determined with allowance for the coupling between colored magnetic moments of quarks, which we have not considered.

It is clear from Fig. 9 that  $(N - \Delta)_2$  and  $(N - \Delta)_2'$  are very close to one another. It may be expected that allowance for the spin-spin interaction (subject to the assumption of a triplet diquark) will have little effect on the predictions of

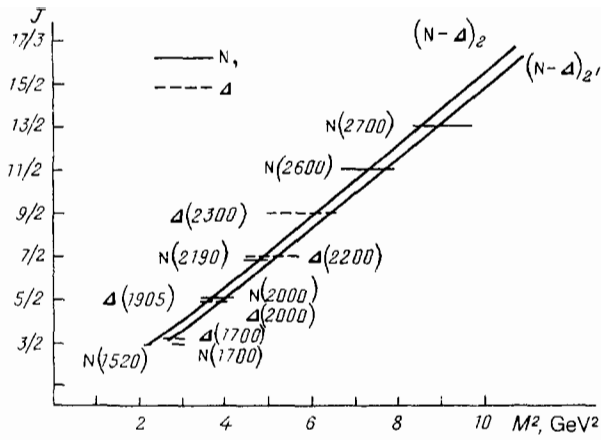


FIG. 9. Masses of orbitally excited baryons  $q - qq$ , with  $J^P = 3/2^-, 5/2^+, \dots, T = 1/2, 3/2$ .

the model. As we have already said, we have neglected configuration mixing because trajectories with singlet and triplet diquarks are well separated. We also note that there is no configuration mixing for the  $\Delta$  resonances. Hence, the degeneracy of the  $N$  and  $\Delta$  trajectories can be regarded as experimental confirmation of the absence of configuration mixing in nucleon resonances. As already noted, this mixing can be seen in the lower excitations ( $J^P = 3/2^-$ ). Figure 9 shows the same resonances as Fig. 8, but with  $J^P = 3/2^-$ . It is clear that they lie between  $N_1$  and  $(N - \Delta)_2$  trajectories. Figure 9 also shows the nucleon resonance  $J^P = 13/2^+$  mentioned earlier.

All that we have said in this Section remains in force for trajectories with the triplet diquark and  $J = l - 1/2$ ,  $J^P = 1/2^-, 3/2^+, 5/2^-$ , and so on. The model predictions and the experimental data are shown in Fig. 10 [( $N - \Delta$ )<sub>3</sub> and ( $N - \Delta$ )<sub>3'</sub> trajectories].

Figure 11 shows the orbital excitations of nucleons containing the singlet diquark. As before, configuration mixing of the lower excitations lying on the ( $N - \Delta$ )<sub>3</sub>, ( $N - \Delta$ )<sub>3'</sub>, and  $N_2$  trajectories is possible (see Figs. 10 and 11). The resonance  $N(1535)$  with  $J^P = 1/2^-$  is therefore shown in both figures. Figure 11 also shows the model predictions for orbitally excited baryons containing the triplet diquark and having spin  $J = l - 3/2$  [( $N - \Delta$ )<sub>4</sub> trajectory]. The  $N$  and  $\Delta$  resonances with quantum numbers  $J^P = 1/2^+, 3/2^-, 5/2^+$ , and so on should lie on this trajectory.

The trajectories shown in Figs. 7-11 are thus seen to

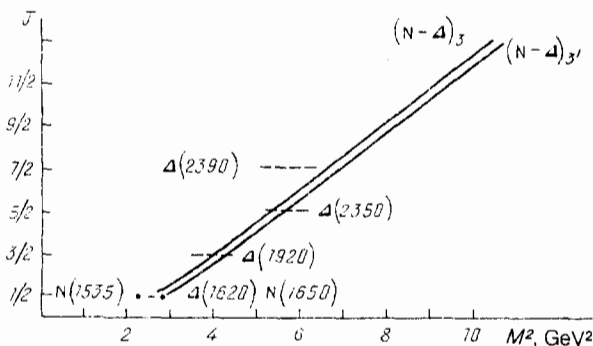


FIG. 10. Masses of orbitally excited baryons  $q - qq$ , with  $J^P = 1/2^-, 3/2^+, \dots, T = 1/2, 3/2$ .

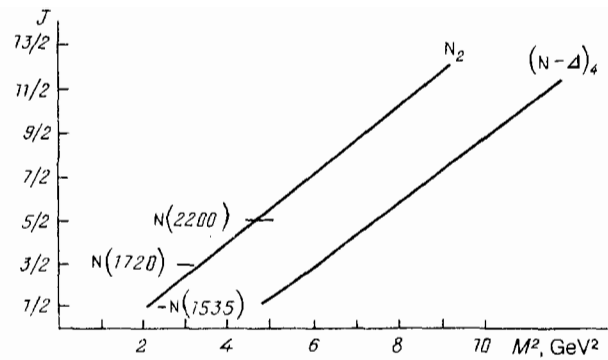


FIG. 11. Masses of orbitally excited baryons  $q - qq_0$  with  $J^P = 1/2^-, 3/2^+, \dots, T = 1/2$  (trajectory  $N_2$  and  $q - qq_1$  with  $J^P = 1/2^+, 3/2^-, \dots, T = 1/2, 3/2$  trajectory  $(N - \Delta)_4$ ).

exhaust the model predictions for the spectrum of baryon resonances that constitute orbital excitations in the system of three nonstrange quarks.

#### 4.5. The spectrum of $\Lambda$ hyperons

We now turn to strange baryons. The first interesting feature is the spectrum of orbital excitations of  $\Lambda$  hyperons. We have already shown that the energetically most favorable configuration is a string with a quark and a diquark at the ends. Since the  $\Lambda$  hyperon consists of  $u, d$ , and  $s$  quarks and has isospin 0, the possible subdivisions into color clusters as a result of orbital excitation are as follows:

- a)  $s - ud$  ( $T = S = 0$ ),
- b)  $q - qs$  ( $T = 1/2, S = 0$ ),
- c)  $q - qs$  ( $T = 1/2, S = 1$ ) ( $q = u, d$ ).

In actual fact, physical particles can look like superpositions of states corresponding to these subdivisions, especially if the masses of the different diquarks are close to one another. However, the properties of  $N$  and  $\Delta$  trajectories show that the singlet diquark is significantly lighter than the triplet diquark. It follows that the configuration  $s-ud$  ( $S = T = 0$ ) may well be favored and that the lowest levels in the spectrum of  $\Lambda$  hyperons will have a small admixture of other configurations. If this is indeed the case, then we can predict the mass spectrum of orbital excitations of  $\Lambda$  particles without introducing new parameters. All that needs to be done is to make the following substitutions in (4.1)-(4.3):

$$\mu_1 = m_s, \quad \mu_2 = m_0; \quad s_1 = 1/2, \quad s_2 = 0.$$

The results of this are shown in Fig. 12 together with the experimental data. It is clear that there is good agreement, which confirms the above assumptions. The determination of the spectra of other strange baryons will require at the very least the introduction of additional parameters (masses of diquarks with nonzero strangeness).

#### 4.6. Mesons consisting of diquarks

One of the important points in the description of baryon trajectories was the introduction of the diquarks  $qq_0$  and  $qq_1$  into the model. The diquarks were found to be relatively light, and the natural question that has arisen is: what is the mass spectrum of meson states described by a string with diquarks at the ends? The existence of multi-quark hadrons

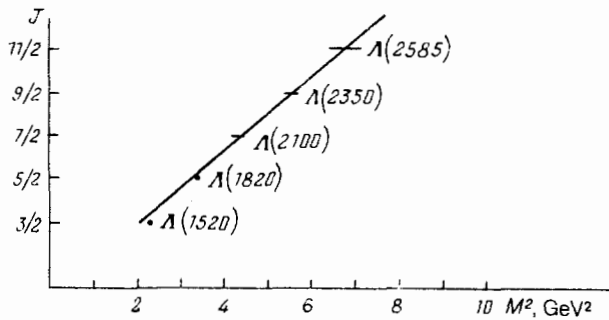


FIG. 12. Orbital excitations of the  $\Lambda$  hyperon with  $J^P = 3/2^-, 5/2^+, \dots$

and, in particular, those with exotic quantum numbers, has been under discussion in the literature for some time (see, for example, Refs. 1 and 26–31). Current candidates for multi-quark hadrons have already come forward, but their status is not entirely clear (see Refs. 1 and 29–31). It may well be that orbitally excited four-quark mesons in which the diquarks are held apart by a centrifugal barrier will become a very effective source of information on multi-quark systems.

In the string model, the masses of the  $qq - \bar{q}\bar{q}$  mesons are predicted unambiguously as soon as the diquark masses are fixed. We recall that we are considering diquarks that are color triplets, so that the string tension  $\nu$  is at a minimum and is equal to the string tension in 'ordinary' mesons.

The spectrum of orbital excitations with singlet diquarks at the string ends can be calculated from (4.1)–(4.3) with

$$\mu_1 = \mu_2 = m_0; \quad s_1 = s_2 = 0.$$

These calculations are shown by trajectory 1 in Fig. 13. States lying on this trajectory have isospin 0. The quantum numbers are  $J^P = 1^{--}, 2^{++}, 3^{--}, \dots$ , and the  $G$ -parity is equal to the  $C$ -parity.

The masses of orbitally excited 4q levels constructed from the singlet and triplet diquarks ( $qq_0 - \bar{q}\bar{q}_1$  and  $qq_1 - \bar{q}\bar{q}_0$ ) can be calculated from the same formulas with

$$\mu_1 = m_0, \quad \mu_2 = m_1; \quad s_1 = 0, \quad s_2 = 1.$$

The numerical results are indicated by trajectory 2 in Fig. 13. The states  $qq_0 - \bar{q}\bar{q}_1$  and  $qq_1 - \bar{q}\bar{q}_0$  (indicated by  $|1\rangle$  and  $|2\rangle$ ) are obviously degenerate. It is also clear that these states do not have specific  $C$  and  $CP$  parities. States with definite  $C$  and  $CP$  are the linear superpositions:

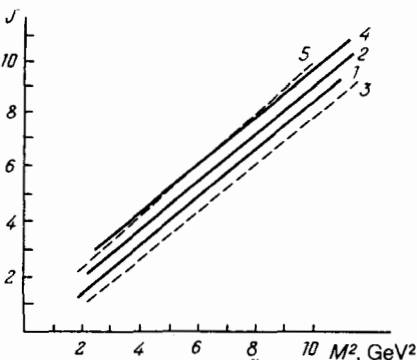


FIG. 13. Orbital excitations of mesons consisting of non-strange diquarks compared with  $q\bar{q}$  excitations (dotted trajectories).

$$|1'\rangle = \frac{1}{\sqrt{2}} (|1\rangle - |2\rangle),$$

$$|2'\rangle = \frac{1}{\sqrt{2}} (|1\rangle + |2\rangle).$$

The diquark isospins are 0 and 1, respectively, so that the total isospin is fixed and equal to 1. The quantum numbers of states of the form  $|1'\rangle$  are  $J^{PC} = 2^{--}, 3^{+-}, 4^{-+}, \dots$  and are equal to the quantum numbers of particles on the  $\pi$  trajectory. States of the form  $|2'\rangle$  have quantum numbers  $J^{PC} = 2^{--}, 3^{++}, 4^{--}, \dots$ . The states  $|1'\rangle$  and  $|2'\rangle$  with different  $C$  parities but the same quantum numbers  $J^P$  are degenerate. The degeneracy can be lifted by the exchange interaction or, for example, by interaction with open hadron channels because of the different  $C$ , i.e., different  $G$ , parities. For comparison, Figure 13 also shows the  $\pi$  trajectories (dashed trajectory 3). It is interesting to note that the resonances on the  $\pi$  trajectory are somewhat heavier than the 4q states with the same quantum numbers  $J^P$  (cf. trajectories 2 and 3 in Fig. 13).

Finally, consider mesons consisting of triplet diquarks. The masses of the states with the energetically most favorable orientation of diquark spins can be calculated from (4.1)–(4.3) in which

$$\mu_1 = \mu_2 = m_1, \quad s_1 = s_2 = 1$$

(trajectory 4 in Fig. 13). The total isospin can be  $T = 0, 1$ , or 2. In our model, these states are degenerate. The quantum numbers are  $J^{PC} = 3^{--}, 4^{++}, 5^{--}, \dots$  and are the same as on the  $\rho$  trajectory (trajectory 5). It is clear that trajectories 4 and 5 are practically identical, and that the separation between particles with the same  $J$  does not exceed 20 MeV for high orbital excitations.

This is how the model predictions look in relation to the masses of states with the energetically most favorable orientations of diquark spins in  $ls$ -coupling. Particles constructed from triplet diquarks  $qq_1 - \bar{q}\bar{q}_1$  are the lightest for given spin  $J$ .

They include particles with isospin  $T = 2$ , and it would be interesting to verify the existence of such particles experimentally.

Apart from the results given above, the model offers a number of further predictions characterized by different diquark spin orientations relative to the direction of  $\mathbf{l}$ , so that the corresponding masses are different by an amount equal to the spin-orbit interaction energy (cf. Ref. 32). Comparisons with other models and a discussion of the relation to the baryonium problem are also presented in Ref. 32. It is clear from the above results that the model predicts a large number of boson resonances near and above the  $N\bar{N}$  threshold. We also note that many of the predicted resonances lie below this threshold. The lightest of them is the meson constructed from singlet diquarks with  $I^G(J^{PC}) = 0^-(1^{--})$  and masses in the range 1.2–1.3 GeV.

The  $C$ -meson with hidden strangeness was discovered relatively recently<sup>33</sup> and was found to decay along the  $\varphi\pi^0$  channel and to have quantum numbers  $J^P = 1^-$ . The mass of this meson is  $m_C = 1480$  MeV. It was described in Ref. 33 as a four-quark object of the form  $q\bar{q}s\bar{s}$ . In the string model, this meson can be interpreted as the first orbital excitation of the system consisting of strange diquarks with zero spins, i.e.,  $qs_0 - \bar{q}\bar{s}_0$ . If this is so, then this experiment can be used

to determine the mass of the strange diquark and to predict the masses of higher orbital excitations. The mass of  $qs_0$  turns out to be 360 MeV, which is greater by 140 MeV than the mass of the nonstrange quark  $qq_0$  (we recall that, in our model, the effective masses of the strange and nonstrange quarks differ by 100 MeV). The masses of the next orbital excitations on the C-meson trajectory are  $2^+$  (1.88 GeV),  $3^-$  (2.19 GeV), and  $4^+$  (2.46 GeV). According to our model, particles with isospin 0 should lie at the same points.

#### 4.7. Dibaryons

There are many reasons why it is interesting to consider orbital excitations of six-quark states. First, the ground states of these systems are relatively heavy because of the strong spin-spin repulsion between the quarks and the possible increase in the constant  $B$ , i.e., the vacuum energy density.<sup>34-40</sup> Second, these states should readily decay into open hadronic channels and are therefore relatively wide. The division of  $6q$  systems into clusters, e.g., by the centrifugal barrier, should therefore be favorable from both the energy point of view and from the point of view of stability against decay into colorless hadrons.

Orbital excitation of  $6q$  systems were considered earlier in Ref. 37. The new point in our discussion is the inclusion of the spin-orbit interaction of clusters. It turns out that the spin-orbit interaction not only provides a correction to the energy of the rotating dibaryon, but also determines the choice of the energetically favorable subdivision into quark clusters.

An analysis of the relatively well-known rotational series of dibaryons  ${}^3F_3(2.25)$ ,  ${}^1G_4(2.43)$ ,  ${}^3H_5(2.7)$ ,  ${}^1I_6(2.9)$ ,... was used in Ref. 41 to show that the most favorable configuration was the diquark  $qq_1$  and the four-quark cluster  $q_{01}^4$  with  $T = 0$  and  $S = 1$  (Fig. 14). The mass of the cluster  $q_{01}^4$  was found to lie in the range 1.05–1.15 GeV.

By replacing the diquark  $qq_1$  with  $qq_0$  we obtain a series of dibaryons with  $T = 0$ . The lowest state in this series,  $d'$ , has  $l = 1$  and  $J^P = 2^-$ . It is relatively light, i.e.,  $m(d') = 1.95$ – $2.05$  GeV. It is important to note that this dibaryon cannot decay in the  $NN$  channel because of its quantum numbers. The principal decay channel is therefore  $NN\pi$ . However, this also is possible only if the  $d'$  lies above the  $NN\pi$  threshold (2.02 GeV). When this is not so, the principal decay mode is electromagnetic, i.e.,  $d' \rightarrow d\gamma$ . Figure 14 shows the predictions for the remaining orbital excitations on the  $d'$  trajectories.

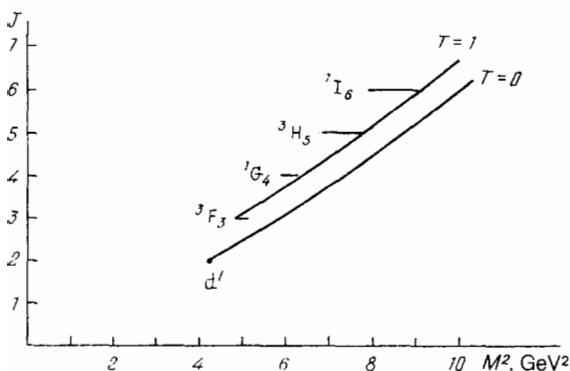


FIG. 14. Orbital excitations with double the baryon charge.

### 5. LOW VALUES OF $J$ . MODEL-INDEPENDENT ANALYSIS OF P-WAVE HADRONS. THE SPECTRA OF MESONS CONSISTING OF A LIGHT AND A HEAVY QUARK

For low orbital excitations, the quark spin precession is influenced both by the Thomas effect and by the chromomagnetic field due to the presence of the vector interaction between quarks and the induced chromoelectric field (see §1). We shall now use the language of potential models<sup>42,43</sup> to estimate the contribution of different spin effects, taking P-wave mesons as an example. With these estimates as the starting point, we can try to predict the values of  $l$  for which there should be a transition to a reversed level ordering (as compared with the Coulomb case), with the  $l$ -splitting dominated by the Thomas effect. Mesons constructed from a light and a heavy quark occupy a special place from this point of view. Once we know the different spin-dependent contributions, we can interpret the details of the spectrum of P-wave  $\Delta$  resonances, having first found the effective Hamiltonian for the interaction between the quark and the triplet diquark.

We start with the fact that the masses of P-wave hadrons can be calculated as follows. First, by solving the wave equation, we find the center of the multiplet and then, as corrections, we calculate the spin splittings on the assumption of the same coordinate dependence of P-level wave functions (actually, a weaker assumption is sufficient: it is enough to assume equal matrix elements of operators that appear in the effective Hamiltonian, and determine the contributions of tensor and spin-orbit forces). The second part of the problem can be treated separately in a model-independent manner, i.e., without using any specific wave functions.

#### 5.1. Spin effects in the spectra of P-wave mesons

The spin-dependent effective Hamiltonian obtained from QCD in Ref. 44 can be written in the following form when the Lorentz invariance is taken into account:<sup>45</sup>

$$H_s = -\frac{1}{r} \frac{\partial V_1}{\partial r} \left( \frac{s_1}{2m_1^2} + \frac{s_2}{2m_2^2} \right) \mathbf{1} + \frac{1}{r} \frac{\partial V_2}{\partial r} \left( \frac{s_1}{2m_1^2} + \frac{s_2}{2m_2^2} + \frac{s_1 + s_2}{m_1 m_2} \right) \mathbf{1} + \frac{1}{m_1 m_2 r^3} \frac{\partial V_3}{\partial r} ((s_1 r)(s_2 r) - \frac{1}{3} r^2 (s_1 s_2)) + \frac{4}{m_1 m_2 r} \frac{\partial V_4}{\partial r} (s_1 s_2) \quad (5.1)$$

(we note that allowance for the color structure in the case of  $q\bar{q}$  is a trivial problem; the corresponding factors are included in  $V_i$ ). This expression contains terms of the order of  $(v/c)^2$  and is written in the center of mass system of the quarks. The quantities  $s_{1,2}$  and  $m_{1,2}$  are the spins and the effective masses of  $q$  and  $\bar{q}$ , respectively. The Hamiltonian (5.1) has a simple interpretation if we consider that the attraction between  $q$  and  $\bar{q}$  is due to vector (short range) and scalar (string simulating) interactions, and if we also include the induced chromomagnetic field (see §1). Actually, the Thomas precession that includes contributions due to the vector and scalar potentials has an associated energy proportional to

$$\left( \frac{s_1}{2m_1^2} + \frac{s_2}{2m_2^2} \right) \mathbf{1}. \quad (5.2)$$

The chromomagnetic field due to the vector interaction and the presence of induced charges and (or) monopole currents influences the spins of  $q$  and  $q\bar{q}$  and produces  $ls$ -coupling of the form

$$\left(\frac{1}{m_1} + \frac{1}{m_2}\right) \left(\frac{\mathbf{s}_1}{m_1} + \frac{\mathbf{s}_2}{m_2}\right) \cdot \mathbf{l}. \quad (5.3)$$

The total contribution of  $ls$ -dependent corrections can obviously be written in the form of the sum of the first two terms in (5.1). The remaining two are the tensor and spin-spin forces. We note that the induced field ensures that the simple coupling between  $\partial V_i / \partial r$ , which occurs at the level of the tree approximation in the ordinary potential approach (Breit's formula), is now absent. This coupling can also be broken by the  $\alpha_3$  corrections to the effective potential  $V_i$ , which cannot be regarded as small<sup>46</sup> for the  $q\bar{q}$  mesons ( $q = u, d$ ). In the QCD-based formalism,<sup>44</sup> the coupling between  $\partial V_i / \partial r$  is generally absent. In principle, this coupling could be established by using the approach developed in Refs. 47 and 48.

To proceed from the Hamiltonian (5.1) to the mass formulas, we use the following notation for the matrix elements  $\langle (1/r) \partial V_i / \partial r \rangle$ :

$$\begin{aligned} \left\langle \frac{1}{r} \frac{\partial V_1}{\partial r} \right\rangle &= S, & \left\langle \frac{1}{r} \frac{\partial V_2}{\partial r} \right\rangle &= V, \\ \left\langle \frac{1}{r} \frac{\partial V_3}{\partial r} \right\rangle &= t, & \left\langle \frac{1}{r} \frac{\partial V_4}{\partial r} \right\rangle &= h, \end{aligned} \quad (5.4)$$

and assume that  $S, V, t, h$  are adjustable parameters. It is implied that the color structure has been taken into account and the corresponding factors are included in  $V_i$ . This is a trivial problem in the case of mesons (see §1), but this cannot be said about baryons which will be discussed later.

To fix the parameters, we start with the following traditional particle identification in terms of the quantum numbers of the  $q\bar{q}$  pair (we use the particle notation adopted in the 1990 tables given in Ref. 1):

$$a_2, K_2^*, {}^3P_2, a_1, {}^3P_1, b_1, {}^1P_1, a_0, {}^3P_0,$$

$K_1(1270)$  and  $K_1(1400)$  – mixture of  ${}^3P_1$  and  ${}^1P_1$ .

It is important to note that this interpretation gives rise to a number of problems and that other possibilities are discussed in the literature (see, for example, Ref. 29).

As a preliminary step, we note that the P-wave meson wave function vanishes at the origin and is localized for  $r > 1$  fm. The magnitude of the scalar potential  $kr$  ( $k \sim 1/4$  GeV)<sup>2</sup> that simulates the string in this region, and appears in the wave equation as part of the combination  $m_i + kr_i$ , exceeds the effective mass of the quark  $m_i \sim 1/3$  GeV by a factor of at least 2, whereas the scalar attraction acting on the quarks is stronger than the vector attraction by a factor of at least 2 (Refs. 49 and 50). We can therefore consider that the P-wave wave function and, together with it, the matrix elements  $S, V$ , and  $t$  change very little between nonstrange and strange mesons (which means that one of the masses must increase by about 100 MeV). The dependence of spin splittings on the quark masses is then essentially given by (5.1). This means that the same model-independent approach to the description of spin effects can be used for P-wave  $q\bar{q}$  ( $q = u, d$ ) and  $q\bar{s}$  mesons.

Comparison of the center of the  ${}^3P_J$  multiplet

$$\epsilon = \sum_{J=0}^2 (2J+1) m({}^3P_J) / \sum_{J=0}^2 (2J+1) \quad (5.5)$$

with the mass of the  ${}^1P_1$  meson shows that spin-spin forces are small. We shall therefore assume henceforth that  $h = 0$ . The masses can be readily found from

$$m = \epsilon + \alpha(s_2 - s_1)l + \beta(s_2 + s_1)l + \gamma \hat{T}, \quad (5.6)$$

which follows from (4.10) where

$$\begin{aligned} \alpha &= (S - V)(m_1^{-1} - m_2^{-1})/4, \\ \beta &= (V/m_1 m_2) - [(S - V)(m_1^{-2} + m_2^{-2})/4], \\ \gamma &= t/m_1 m_2 \end{aligned} \quad (5.7)$$

and  $l, s_i$  are interpreted as the matrix elements of the corresponding operators. The contribution of tensor forces can now be calculated with the help of the formula

$$\begin{aligned} \hat{T} &= (2l - 1)^{-1} (2l + 3)^{-1} [-(ls)^2 - \frac{1}{2}(ls) + \frac{1}{3}l^2 s^2], \\ s &= s_1 + s_2. \end{aligned} \quad (5.8)$$

It follows from (4.14)–(4.17) that the P-wave masses are

$$\begin{aligned} m({}^1P_1) &= \epsilon, \\ m({}^3P_2) &= \epsilon + \beta - (\gamma/30), \\ m({}^3P_1) &= \epsilon - \beta + (\gamma/6), \\ m({}^3P_0) &= \epsilon - 2\beta - (\gamma/3). \end{aligned} \quad (5.9)$$

The parameters  $\beta$  and  $\gamma$  are different for strange and nonstrange mesons, and are expressed in terms of the matrix elements  $S, V$ , and  $t$ . In addition, the mixing of axial mesons occurs in the strange sector. The physical states

$$\begin{aligned} |K_1\rangle &= |{}^3P_1\rangle \cos \varphi + |{}^1P_1\rangle \sin \varphi, \\ |K_1'\rangle &= -|{}^3P_1\rangle \sin \varphi + |{}^1P_1\rangle \cos \varphi \end{aligned} \quad (5.10)$$

have masses  $\mu_1$  and  $\mu_2$  that are the eigenvalues of the mass matrix

$$\begin{pmatrix} m({}^3P_1) & \langle {}^3P_1 | H_s | {}^1P_1 \rangle \\ \langle {}^1P_1 | H_s | {}^3P_1 \rangle & m({}^1P_1) \end{pmatrix}, \quad (5.11)$$

where  $\langle {}^3P_1 | H_s | {}^1P_1 \rangle = \alpha\sqrt{2}$  [see (5.6) and (5.7)]. The definition of the mixing angle  $\varphi$  is the same as the definition given in Ref. 51 if  $K_1$  is identified with  $K_1(1400)$  and  $K_1'$  with  $K_1(1270)$ ; the definition corresponding to  $\varphi \rightarrow (\pi/2) - \varphi$  is used in Ref. 52.

Without going into the details of the fit, we reproduce the parameter values that determine the spin splitting of the P-levels: for  $m_s/m_q = \sqrt{2}$

$$S/m_q^2 = 570 \text{ MeV}, \quad V/m_q^2 = 250 \text{ MeV}, \quad t/m_q^2 = 200 \text{ MeV}. \quad (5.12)$$

Table I lists the corresponding mass splittings and the values of  $\varphi$  [for convenience, we reproduce the masses themselves, having fixed the position of the centers of the multiplets  $q\bar{q}$  and  $q\bar{s}$  in accordance with the mass of the  $b_1$  meson

TABLE I. Mesons (masses in MeV).

	$a_0$	$a_1$	$b_1$	$a_2$	$K_0$	$K_1'$	$K_1$	$K_2$	$\varphi$
Model	983	1173	1230	1313	1191	1276	1394	1404	53,5°
Experi- ment	983 ± 3	1262 ± 23	1232,6 ± 3,0	1310,7 ± 1,3		1270 ± 10	1401 ± 10	1425,6 ± 1,5	56° ± 3°

and the half-sum of the masses of  $K_1$  (1270) and  $K_1$  (1400), respectively]. It is clear that this model-independent approach allows us to describe the masses of P-wave mesons to within at least 20 MeV with the exception of the mass of  $a_1$ , which is approximately 80 MeV below the tabulated value.<sup>1</sup> Problems associated with the determination of the position of the  $a_1$  resonance are discussed in a number of papers (cf. Ref. 53 and the bibliography in Ref. 1) and can hardly be regarded as finally settled. We also draw attention to the prediction of the scalar  $K_0^*$  meson ( $J^P = 0^+$ ) with a mass of 1.2 MeV (the analog of  $a_0$ ). This particle has not been discovered as yet, and the lightest of all the known scalar kaons is  $K_0^*$  (1350), which clearly cannot be interpreted as the lowest  $^3P_0$  state.

An analysis of the spin splittings of P-mesons (including mesons consisting of heavy quarks) was also performed in Ref. 54 (see also Ref. 55) on the basis of the tree approximation for the effective Hamiltonian. The estimated matrix elements of the scalar and vector interactions are very different from those obtained above [see (5.12)] and lead to significant discrepancies from experimental data on K-mesons. However, in their final answer, the authors of Ref. 54 use a different parametrization that satisfies the empirical dependence found by them of the matrix elements  $\langle r^{-1} \partial V_i / \partial r \rangle$  on the quark masses in a broad range of mass values (right up to the b quark). However, this parametrization produces considerable discrepancies from experimental data on  $q\bar{q}$  and  $q\bar{s}$  mesons (see Table IV in Ref. 54).

It follows from our calculations that the splitting of the P-levels is largely due to  $ls$ -forces. The separate contribution of the vector and scalar interactions (e.g., to the mass difference between  $^3P_2$  and  $^3P_0$  levels) is of the order of 1 GeV, whereas the P-wave is dominated by the vector interaction and the resultant effect is  $\sim 300$  MeV. A similar picture emerges in the spectrum of P-wave  $\Delta$  resonances whose masses can be estimated with the same  $S$ ,  $V$ , and  $t$ .

### 5.2. P-levels of the $\Delta$ isobar

From the standpoint of the model-independent analysis, the first orbital excitation of negative-parity  $\Delta$  baryons is the simplest of all the excited analogs of light baryons, namely, the  $3q$  system. Such levels can be looked upon as P-waves in the two-particle quark plus triplet diquark system. There are obviously five such levels:  $^4P_J$  ( $J = 1/2, 3/2, 5/2$ ) and  $^2P_J$  ( $J = 1/2, 3/2$ ). Each physical particle with  $J = 3/2$  and  $1/2$  has its own superposition of states with total quark spin  $1/2$  or  $3/2$ , determined by the spin-orbit as well as tensor forces. To obtain numerical predictions, we must specify the mass and the colored magnetic moment of the triplet diquark. We shall assume, following the additive quark model, that

$$\vec{\mu}_{qq}^a = \frac{s_1}{m_1} \frac{\lambda_1^a}{2} + \frac{s_2}{m_2} \frac{\lambda_2^a}{2}, \quad (5.13)$$

and that the mass of the diquark  $m_{qq}$  is of the order of twice

the mass of the quark (subscripts 1 and 2 label the two quarks in the diquark). The form of the  $ls$ -interaction can be readily established by analogy with  $q\bar{q}$ . We need only remember that the energy of interaction between the chromomagnetic moment of the 'isolated' quark and the resultant magnetic field is proportional to

$$s_3 \lambda_3^a (\lambda_1^a + \lambda_2^a) l,$$

whereas the analogous quantity for the diquark is

$$\lambda_3^a (s_1 \lambda_1^a + s_2 \lambda_2^a) l.$$

Hence, it is clear that the spins  $s_1$  and  $s_2$  of the quarks in the diquark appear with the coefficient  $1/2$  as compared with the spin  $s_3$  of the 'isolated' quark.

The Thomas spin precession can be taken into account by analogy with  $q\bar{q}$ , and the corresponding energy term is obtained by substituting

$$s_1 \rightarrow s_1 + s_2, \quad s_2 \rightarrow s_3$$

in (5.1).

Finally, the contribution of the tensor forces is also readily found from the corresponding term in (5.10) with

$$s_1 \lambda_1^a / m_1 \rightarrow s_1 \lambda_1^a / m_q + s_2 \lambda_2^a / m_q, \quad s_2 \lambda_2^a / m_2 \rightarrow s_3 \lambda_3^a / m_q.$$

If we combine all these contributions and substitute explicitly for the matrix element  $\lambda_i^a \lambda_k^a$ , we obtain the following expression for the spin-dependent energy of interaction between the quark and the triplet diquark with relative orbital angular momentum  $l$ :

$$\begin{aligned} H_s^{(\Delta)} = & -\frac{1}{r} \frac{\partial V_1}{\partial r} \left[ \frac{s_{qq}}{2m_{qq}^2} + \frac{s_q}{2m_q^2} \right] l \\ & + \frac{1}{r} \frac{\partial V_2}{\partial r} \left[ \left( \frac{s_{qq}}{2} + s_q \right) (m_q^{-1} + m_{qq}^{-1}) m_q^{-1} - \frac{s_{qq}}{2m_{qq}^2} - \frac{s_q}{2m_q^2} \right] l \\ & + \frac{1}{2r^3 m_q^2} \frac{\partial V_3}{\partial r} [ (s_{qq} r)(s_q r) - \frac{1}{3} (s_q s_{qq}) r^2 ] \quad (5.14) \end{aligned}$$

where  $s_{qq} = s_1 + s_2$ ,  $s_q = s_3$ . This formula readily yields the form of the  $ls$ -interaction in the system consisting of a quark and a single diquark if we substitute  $s_{qq} = 0$  and assume that  $m_{qq}$  is the effective mass of the singlet diquark.

We now turn to the evaluation of the spin-splittings of the masses of  $\Delta$  excitations, using the matrix elements  $\langle r^{-1} \partial V_i / \partial r \rangle$  found from the meson spectrum. As before, the tensor contributions can be calculated from the formula

$$\hat{T} = (2l - 1)^{-1} (2l + 3)^{-1} [ -\{ (ls_q), (ls_{qq}) \}_+ + \frac{2}{3} l^2 (s_q s_{qq}) ] \quad (5.15)$$

where  $\langle \dots \rangle_+$  is the anticommutator. However, this formula does not now reduce to the expression in terms of the total quark spin operator. For the maximum possible  $J = 5/2$ , we have

$$m(^4P_{3/2}) = \epsilon_\Delta + \frac{1}{4m_q^2} [V(3 + 4x - 2x^2) - S(1 + 2x^2)] - \frac{t}{30m_q^2}, \quad x = \frac{m_q}{m_{qq}}, \quad (5.16)$$

where  $\epsilon_\Delta$  is the center of the multiplet.

Each of the  $J = 3/2$  states (we shall denote them by  $\Delta_{3/2}$  and  $\Delta'_{3/2}$ ) is a superposition of  $^4P_{3/2}$  and  $^2P_{3/2}$  states (by analogy with the mixing of  $^1P_1$  and  $^3P_1$  in K mesons) and their masses are the eigenvalues of the mass matrix  $\|\mu_{ik}\|$  where

$$\begin{aligned} \mu_{11} &= m(^4P_{3/2}), \quad \mu_{22} = m(^2P_{3/2}), \\ \mu_{12} &= \langle ^4P_{3/2} | H_s^{(\Delta)} | ^2P_{3/2} \rangle = \mu_{21}^*. \end{aligned} \quad (5.17)$$

This also applies to states with  $J = 1/2$  ( $\Delta_{1/2}$  and  $\Delta'_{1/2}$ ). The off-diagonal elements of  $\|\mu_{ik}\|$  are determined not only by the spin-orbit, but also the tensor part of  $H_s^{(\Delta)}$ . Details can be found in Ref. 50 and we reproduce only the final result. For  $J = 3/2$

$$\begin{aligned} \mu_{11} &= \epsilon_\Delta - \frac{1}{6m_q^2} [V(3 + 4x - 2x^2) - S(1 + 2x^2)] + \frac{2}{15} \frac{t}{m_q^2}, \\ \mu_{22} &= \epsilon_\Delta + \frac{1}{12m_q^2} [V(3 + 2x - 4x^2) - S(4x^2 - 1)], \\ \mu_{12} &= \frac{\sqrt{5}}{6m_q^2} [V(x + x^2) - S(1 - x^2)] - \frac{\sqrt{5}}{60} \frac{t}{m_q^2}. \end{aligned} \quad (5.18)$$

For  $J = 1/2$

$$\begin{aligned} \mu_{11} &= m(^4P_{1/2}) \\ &= \epsilon_\Delta - \frac{5}{12m_q^2} [V(3 + 4x - 2x^2) - S(1 + 2x^2)] - \frac{t}{6m_q^2}, \\ \mu_{22} &= m(^2P_{1/2}) = \epsilon_\Delta - \frac{1}{6m_q^2} [V(3 + 2x - 4x^2) - S(4x^2 - 1)], \\ \mu_{12} &= -\frac{\sqrt{2}}{6m_q^2} [V(x + x^2) - S(1 - x^2)] - \frac{\sqrt{2}}{12} \frac{t}{m_q^2}. \end{aligned} \quad (5.19)$$

The spin splittings can now be calculated by substituting the values of  $V$ ,  $S$ , and  $t$  found in the last Section in (4.25)–(4.28), and taking  $x = m_q/m_{qq} = 1/2$ .

Anticipating a little, we note that all the experimentally established<sup>1</sup> lightest negative-parity  $\Delta$  resonances can be identified as P-wave excitations of  $\Delta$ . A clearer picture of the results emerges if we fix the center of the multiplet with the help of the formula

$$\epsilon_\Delta = \sum_J (2J + 1) m(^{2s+1}P_J) \left[ \sum_J (2J + 1) \right]^{-1}, \quad s = \frac{1}{2}, \frac{3}{2}. \quad (5.20)$$

Since the sum  $m(^4P_J) + m(^2P_J)$  is equal to the sum of the masses of the diagonal states for each of the possible values of  $J$  (1/2, 3/2),  $\epsilon_\Delta$  can be readily expressed in terms of the

masses of the physical states by introducing in addition a summation over  $s$ . These calculations are summarized in Table II. It is clear that there is relatively good agreement with experiment with the exception of the mass of  $\Delta'_{3/2}$ . Better agreement can be achieved by varying the ratio  $m_q/m_{qq}$ . However, no less important is the fact that the model-independent description predicts the experimentally observed relative position of P-levels. We note that the main contribution to the level splitting comes from the spin-orbit interaction. The  $ls$ -coupling was totally ignored in Ref. 56, and all the splittings in orbitally excited hadrons were described by tensor forces. The motivation for this was that the  $ls$  contributions of the vector and scalar potentials practically cancelled out. It is clear from (5.16)–(5.19) that this is simply not possible for all the P-levels. Moreover, the calculations reported in Ref. 56 did not cover all the negative-parity levels.

### 5.3. Orbital angular momenta $l > 1$ . Mesons consisting of a light and a heavy quark

As the orbital angular momentum increases, the contribution of the vector interaction decreases much more rapidly than the contribution of the long-range part of the effective potential  $H_s$ . The spin splittings are then dominated by the Thomas effect. Of course, precise predictions based on the model-independent approach are hardly possible, but very approximate estimates show that  $r \sim l^{1/2}$  and that for  $l = 2, 3$  there should already be a transition to the reverse level ordering (as compared with the Coulomb case). Spin orientation along  $l$  is energetically favorable. The experimental situation shows that practically complete cancellation of different spin-dependent contributions occurs in the D-wave analogs of light mesons: the masses of  $\omega_3$ ,  $\rho_3$ , and  $\pi_2$  are practically equal. The reverse level ordering is observed for the F wave (cf. Fig. 1).

The reverse level ordering and the dominance of the Thomas effect for  $l > 2$  are much clearer in kaons (cf. Fig. 2).

It follows from (5.11) that, in mesons consisting of a light and a heavy quark ( $q\bar{Q}$ ), the reverse level ordering should occur for smaller  $l$  (Ref. 57). The properties of the spectrum of orbital excitations of  $q\bar{Q}$  mesons are also discussed in Refs. 58 and 59.

## 6. DECAY OF ORBITALLY EXCITED HADRONS

We shall now briefly discuss certain features of the string-model decay of a hadron, due to the creation of a  $q\bar{q}$  pair in the chromoelectric field of a string.<sup>60–62</sup> We shall be interested mainly in two-particle decay modes.

The basic properties of fragments produced during the rupture of the string can be judged from the simplest version of the model in which the quark masses and spins are not taken into account. As an example, we consider the two-particle decay of a string describing meson excitation.

Suppose that at the time of decay the string lies along the  $x$  axis, the center of rotation lies at the origin, and the axis

TABLE II.  $\Delta$ -resonances (masses in MeV).

	$\Delta_{1/2}$	$\Delta'_{1/2}$	$\Delta_{3/2}$	$\Delta'_{3/2}$	$\Delta_{5/2}$
Model	1660	1730	1747	1958	1891
Experiment	1600 – 1650	1850 – 2000	1630 – 1740	1940	1890 – 1960

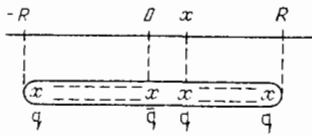


FIG. 15. Decay of an orbitally excited meson resulting in the creation of a  $q\bar{q}$ -pair.

of rotation is parallel to the  $z$  axis. Next, suppose that the production of the  $q\bar{q}$  pair and, correspondingly, the 'rupture' of the string into two fragments occurs at the point  $x$  defined by  $-R < x < R$  (Fig. 15). It is clear *a priori* that this decay can result in hadron states that are mixed orbital-radial excitations. Actually, when the string splits into two parts, unbalanced attractive forces act at the point of rupture and should give rise to radial oscillations. The fraction of energy spent in these radial oscillations and the average spin of a fragment can be determined as follows.

The momentum and energy of a fragment whose extreme points are at  $x$  and  $1/\omega$  are, respectively, given by

$$P = \int_x^{1/\omega} \frac{v\omega x dx}{[1 - (\omega x)^2]^{1/2}} = \frac{v}{\omega} [1 - (\omega x)^2]^{1/2}, \quad (6.1)$$

$$E = \int_x^{1/\omega} \frac{v dx}{[1 - (\omega x)^2]^{1/2}} = \frac{v}{\omega} \arccos(\omega x),$$

where  $\omega = 1/R$  is the angular frequency.

The velocity of the center of mass of the fragment is then given by

$$V = [1 - (\omega x)^2]^{1/2} / \arccos(\omega x). \quad (6.2)$$

The intrinsic angular momentum (spin)  $s$  and the energy  $M$  of the fragment in its rest frame can be calculated from

$$s = \int_x^R \frac{dP - V dE}{(1 - V^2)^{1/2}},$$

and

$$M = \int_x^R \frac{dE - V dP}{(1 - V^2)^{1/2}},$$

where  $V$  is the velocity of the center of mass of the fragment, given by (6.2), and  $dP$  and  $dE$  are the momentum and energy of a string element  $dx$ , respectively. Simple calculations yield

$$s = \frac{v}{\omega^2(1 - V^2)^{1/2}} \left[ \frac{1}{2} \omega x [1 - (\omega x)^2]^{1/2} + \frac{1}{2} \arccos(\omega x) - \frac{1 - (\omega x)^2}{\arccos(\omega x)} \right], \quad (6.3)$$

$$M = \frac{v}{\omega(1 - V^2)^{1/2}} \left[ \arccos(\omega x) - \frac{1 - (\omega x)^2}{\arccos(\omega x)} \right]. \quad (6.4)$$

A fragment is in a state of pure rotational excitation if its mass and intrinsic angular momentum are related by  $M^2 = 2\pi v s$ . Figure 16 shows  $M/M_0$  and  $(2\pi v s)^{1/2}/M_0$ , given by (6.3) and (6.4), as functions of the rupture point ( $M_0$  is the mass of the initial string). It is clear that

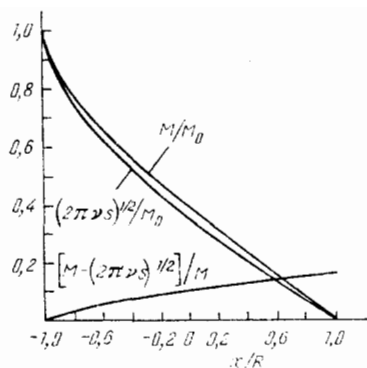


FIG. 16. Mass of a fragment formed in the decay of a string as a function of the point of rupture.

$M > (2\pi v s)^{1/2}$ . The energy excess should be expended in producing radial excitations:

$$\Delta E = M - (2\pi v s)^{1/2}. \quad (6.5)$$

The decay of Regge mesons (if it proceeds in accordance with the above mechanism) should thus lead to the appearance of mixed orbitally-radially excited states. The fraction of fragment energy expended in exciting radial oscillations is small and varies from zero at  $x = -R$  to 0.15 at  $x = R$  (Fig. 16). It amounts to about 0.09 for symmetric decays. We note that the excitation of radial oscillations should lead to an increase in the effective linear energy density  $v$  of the fragment, which is not taken into account in (6.4). This means that the fraction of energy transferred to radial oscillations is actually lower still.

The above model can be used to calculate the fragment spin distribution. We recall that the decay probability within the interval  $dx$  is proportional to  $dx [1 - (\omega x)^2]^{1/2}$ . Figure 17 shows the distribution  $dw/ds$  and the function  $w(s)$ , i.e., the probability that the spin of the resulting fragment is less than  $s$ . The average fragment spin calculated from  $dw/ds$  is 0.17 of the total spin (angular momentum) of the original string. Most of the angular momentum is thus seen to be transferred to the relative orbital angular momentum of the two fragments. The fact that the fragment spin produced by the above decay mechanism is small means that the momenta of the mesons produced during the decay should be largely confined to the plane perpendicular to the spin of the original meson.

We note that, in reality, the angular momentum of both

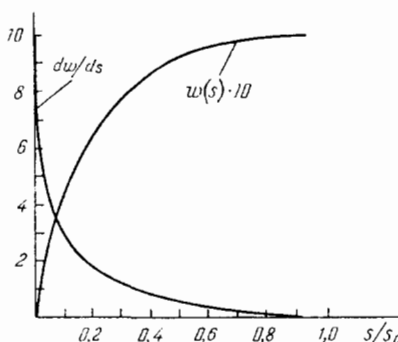


FIG. 17. Functions characterizing the probability of formation of fragments with spin  $s$ .

the original string and of the fragments must of course be a whole number. This in turn means that the distributions that we have given must really be replaced by histograms.

## CONCLUSION

One of the most important problems that arise in any attempt to provide a quasiclassical description of the spectrum of orbital excitations of hadrons is the determination of the spin-orbit interaction. We recall that the choice of the quasiclassical rotator as a model is itself severely limited by the fact that the trajectories are accurately linear for high spins. Our analysis was based on the relativistically invariant QCD-string model. This determines the character of the spin-orbit interaction because only the electric component of the gluon field is then nonzero in the comoving frame, so that the precession of the quark spins is wholly determined by the Thomson effect. The precession frequency can be calculated unambiguously so long as the string rotation dynamics is known. The corresponding energy correction is not small and is comparable, in the region of practical interest, with the separation of neighboring rotational levels corresponding to the same trajectory. It is also important to recall that the model predicts the reverse ordering (as compared with the Coulomb case) of levels differing by the sign of  $\mathbf{l}\cdot\mathbf{s}$ . Of course, all these properties of the spectrum of orbital excitations are typical for sufficiently high orbital excitations. On the other hand, comparison of the model predictions with existing data shows that the model begins to work for angular momenta as low as  $l = 2$  or  $3$ . However, the most important verification of the model and of its predictions relating to  $ls$ -coupling would be the discovery of particles that are spin-orbit splitting partners at higher orbital excitations.

## APPENDICES

1. To find the spin-orbit splitting for a massless fermion confined to a cavity, we have to solve the Dirac equation  $\hat{p}\psi = 0$  with the boundary condition  $i n_\mu \gamma_\mu \psi = \psi$  and compare the energy levels corresponding to wave functions  $\psi_+$  and  $\psi_-$  given by (2.17) for equal values of  $l$

$$\psi_+ \sim \begin{pmatrix} R_l \Omega_{j_+, l} \\ -R_{l+1} \Omega_{j_+, l+1} \end{pmatrix}, \quad \psi_- \sim \begin{pmatrix} R_l \Omega_{j_-, l} \\ -R_{l-1} \Omega_{j_-, l-1} \end{pmatrix}. \quad (\text{A1.1})$$

For  $\psi_+$ , the total angular momentum is  $j_+ = l + 1/2$  and  $\mathbf{l}\cdot\mathbf{s} > 0$ , whereas for  $\psi_-$ , the total angular momentum is  $j_- = l - 1/2$  and  $\mathbf{l}\cdot\mathbf{s} < 0$ . The corresponding energies will be denoted by  $\varepsilon_+$  and  $\varepsilon_-$ , and  $R_l$  will represent spherical Bessel functions. The boundary condition then yields the following equations:

$$R_{l-1}(\varepsilon_- R) = -R_l(\varepsilon_- R), \quad (\text{A1.2})$$

$$R_{l+1}(\varepsilon_+ R) = R_l(\varepsilon_+ R),$$

where  $R$  is the cavity radius.

These equations can be solved<sup>12</sup> for large  $l$ , using the asymptotic expansions for the Bessel functions.<sup>63</sup> The solutions are

$$\varepsilon_+ = \frac{1}{R}(l + C_m l^{1/3} + O(1)), \quad C_m = 0,809, \quad (\text{A1.3})$$

$$\varepsilon_- = \frac{1}{R}(l + C_0 l^{1/3} + O(1)), \quad C_0 = 1,856.$$

The energy difference increases with  $l$  as follows:

$$\varepsilon_- - \varepsilon_+ = \frac{1}{R} C l^{1/3}, \quad C = C_0 - C_m, \quad (\text{A1.4})$$

where the level with parallel  $l$  and  $s$  has the lower energy. The separation between the rotational levels which, we recall, characterizes the rotational frequency for large  $l$ , is given by

$$\Delta\varepsilon_r = \Delta\varepsilon_+ = \Delta\varepsilon_- \approx \frac{1}{R}. \quad (\text{A1.5})$$

The spin-orbit splitting for large  $l$  is thus  $\varepsilon_- - \varepsilon_+ \gg \Delta\varepsilon_r$ . Since we assumed that the fermion mass inside the cavity was initially zero, the effective mass is determined by radial localization. Using the properties of the Bessel functions, we can verify that the fermion wave function is nonzero in a relatively narrow layer near the surface. The layer thickness is  $\Delta R \sim R/l^{2/3}$ . The effective mass of the fermion is therefore  $m_{\text{eff}} \sim l^{2/3}/R$ . The fermion energy is  $\varepsilon_0 \sim 1/R$ , so that  $\gamma = \varepsilon_0/m_{\text{eff}} \sim l^{1/3}$ .

2. We shall now calculate the  $ls$ -splitting for a particle in a scalar field, using the following expression for the square of the Hamiltonian:

$$H^2 = \mathbf{p}^2 + m^2 + im'(\mathbf{n}\boldsymbol{\gamma}), \quad \mathbf{n} = \mathbf{r}/r. \quad (\text{A2.1})$$

The following equations relating the functions  $fg$ ,  $f^2 - g^2$ , and  $f^2 + g^2$  can be readily found from (2.18):

$$fg = \frac{1}{4\varepsilon r^2}(r^2 f^2 - r^2 g^2)' + \frac{\kappa}{2\varepsilon r}(f^2 + g^2), \quad (\text{A2.2})$$

$$f^2 - g^2 = \frac{m}{\varepsilon}(f^2 + g^2) - \frac{1}{\varepsilon r^2}(r^2 fg)'$$

Integrating  $\psi^+ H^2 \psi$  by parts, and using (A2.2), we obtain the following expression for the square of the energy  $\varepsilon^2 = \langle H^2 \rangle$ :

$$\varepsilon^2 = \langle \mathbf{p}^2 + m^2 \rangle - \int \psi^+ \frac{m}{2\varepsilon^2} \left[ m^{(2)} - \frac{m^{(4)}}{4\varepsilon^2} + \frac{m^{(6)}}{(4\varepsilon^2)^2} - \dots \right] \psi d^3r + \int \psi^+ \frac{\kappa}{\varepsilon r} \left[ m' - \frac{m^{(3)}}{4\varepsilon^2} + \frac{m^{(5)}}{(4\varepsilon^2)^2} - \dots \right] \psi d^3r, \quad (\text{A2.3})$$

where  $m^{(k)} = \partial^k m / \partial r^k$ . Most of the dependence on  $\mathbf{l}\cdot\mathbf{s}$  is contained in the last term. As before, we assume that  $\psi$  decreases sufficiently rapidly at infinity. For large  $l$ , the function  $\psi$  is nonzero near  $r = r_0$ , so that the  $ls$ -splitting is given by

$$\Delta\varepsilon_\kappa = \frac{\kappa}{2\varepsilon_0^2 r_0} \left[ m'(r_0) - \frac{m^{(3)}(r_0)}{4\varepsilon_0^2} + \frac{m^{(5)}(r_0)}{(4\varepsilon_0^2)^2} - \dots \right]. \quad (\text{A2.4})$$

For power-type and exponentially growing potentials, (A2.4) gives the following result in the relativistic region:

$$\Delta\varepsilon_{ls} = \gamma\omega, \quad \omega = \Delta\varepsilon_r. \quad (\text{A2.5})$$

The wave function  $\psi$  is also found to depend on  $\mathbf{l}\cdot\mathbf{s}$ . The additional contribution to the  $ls$ -splitting energy therefore arises from the term  $\langle \mathbf{p}^2 + m^2 \rangle$ . This contribution is readily taken into account, and the final result is

$$\Delta\varepsilon_{ls} = (\gamma - 1)\omega. \quad (\text{A2.6})$$

- <sup>1</sup>This also applies to the resonance N(2600); cf. Figs. 8 and 9.
- <sup>2</sup>The quantity  $k$  is fixed quite firmly by the slope of the Regge trajectories because  $M_l^2 \approx 4kl$  for large  $l$  in potential models with linearly rising potential.
- <sup>1</sup>Review of Particle Properties, Phys. Lett. **239** (1990).
- <sup>2</sup>Y. Nambu, Phys. Rev. **D 10**, 4262 (1974).
- <sup>3</sup>G. 't'Hooft, Phys. Scr. **D 25**, 13 (1982).
- <sup>4</sup>I. Yu. Kobzarev and B. V. Martem'yanov, Yad. Fiz. **52**, 296 (1990) [Sov. J. Nucl. Phys. **52**, 296 (1990)].
- <sup>5</sup>L. H. Thomas, Philos. Mag. **3**, 1 (1927).
- <sup>6</sup>V. I. Zakharov, Thesis, MIFI, M., 1963.
- <sup>7</sup>V. B. Berestetskii, E. M. Lifshitz, and L. P. Pitaevskii, *Relativistic Quantum Theory*, part I, Addison-Wesley, Reading, MA, 1971 [Russ. original, Nauka, M., 1968].
- <sup>8</sup>A. Chodos *et al.*, Phys. Rev. **D 9**, 3471 (1974).
- <sup>9</sup>A. T. Aerts and L. Heller, *ibid.* **D 23**, 185 (1981).
- <sup>10</sup>C. Rosenzweig, Preprint NSF-ITP 88-19.
- <sup>11</sup>A. Chodos and C. B. Thorn, Nucl. Phys. **B 72**, 509 (1974).
- <sup>12</sup>Yu. I. Kobzarev, B. V. Martem'yanov, and M. G. Shchepkin, Yad. Fiz. **44**, 475 (1986) [Sov. J. Nucl. Phys. **44**, 306 (1986)].
- <sup>13</sup>F. A. Berezin and M. S. Marinov, Pis'ma Zh. Eksp. Teor. Fiz. **21**, 678 (1975) [JETP Lett. **21**, 320 (1975)].
- <sup>14</sup>F. A. Berezin and M. S. Marinov, Ann. Phys. **104**, 336 (1977).
- <sup>15</sup>B. V. Martem'yanov and M. G. Shchepkin, Yad. Fiz. **49**, 708 (1989) [Sov. J. Nucl. Phys. **49**, 438 (1989)].
- <sup>16</sup>B. V. Martem'yanov and M. G. Shchepkin, Yad. Fiz. **45**, 302 (1987) [Sov. J. Nucl. Phys. **45**, 189 (1987)].
- <sup>17</sup>P. J. Mulders, A. T. Aerts, and J. J. De Swart, Phys. Rev. **D 19**, 2635 (1979).
- <sup>18</sup>R. D. Pisarski and J. D. Stark, Nucl. Phys. **B 286**, 657 (1987).
- <sup>19</sup>K. Kikkarwa, T. Kotani, M. Sato, and M. Kenmoku, Phys. Rev. **D 18**, 2606 (1978).
- <sup>20</sup>W. A. Bardeen *et al.*, *ibid.* **D 13**, 2364 (1976); **D 14**, 2193 (1976); I. Bars and A. J. Hanson, *ibid.* **D 13**, 1744.
- <sup>21</sup>V. I. Borodulin, M. S. Plyuschai, and G. P. Pronko, Z. Phys. **C 41**, 293 (1988); V. I. Borodulin, O. L. Zorin, G. P. Pron'ko, A. V. Razumov, and L. D. Solov'yev, Preprint IFVE 84-202, Serpukhov, 1984.
- <sup>22</sup>G. P. Pron'ko, A. V. Razumov, and L. D. Solov'ev, Preprint IFVE 85-74, Serpukhov, 1985.
- <sup>23</sup>I. Yu. Kobzarev *et al.*, Yad. Fiz. **45**, 526 (1987) [Sov. J. Nucl. Phys. **45**, 330 (1987)].
- <sup>24</sup>A. Martin, Preprint CERN-TH 4259, Geneva, 1985.
- <sup>25</sup>A. B. Kaïdalov and A. F. Nilov, Yad. Fiz. **41**, 768 (1985) [Sov. J. Nucl. Phys. **41**, 490 (1985)].
- <sup>26</sup>R. L. Jaffe, Phys. Rev. **D 15**, 267, 281 (1977).
- <sup>27</sup>T. Barnes, Preprint RAL-85-005-1985.
- <sup>28</sup>R. P. Bickerstaff, Philos. Trans. R. Soc. London **A 309**, 611 (1983).
- <sup>29</sup>N. N. Achasov, S. A. Aryanin, and G. N. Shestakov, Usp. Fiz. Nauk **142**, 361 (1984) [Sov. Phys. Usp. **27**, 161 (1984)].
- <sup>30</sup>E. P. Shabalin, Yad. Fiz. **40**, 262 (1984) [Sov. J. Nucl. Phys. **40**, 166 (1984)].
- <sup>31</sup>E. P. Shabalin, Pis'ma Zh. Eksp. Teor. Fiz. **42**, 111 (1985) [JETP Lett. **42**, 135 (1985)].
- <sup>32</sup>L. A. Kondratyuk, B. V. Martem'yanov, and M. G. Shchepkin, Yad. Fiz. **46**, 1552 (1987) [Sov. J. Nucl. Phys. **46**, 921 (1987)].
- <sup>33</sup>S. I. Bitjukov *et al.*, Preprint IHEP 86-110, Serpukhov, 1986.
- <sup>34</sup>A. Yokosawa, Phys. Rep. **64**, 47 (1984).
- <sup>35</sup>M. M. Makarov, Fiz. Elem. Chastits At. Yadra **15**, 941 (1984) [Sov. J. Part. Nucl. **15**, 419 (1984)].
- <sup>36</sup>T. A. De Grand *et al.*, Phys. Rev. **D 12**, 2060 (1975).
- <sup>37</sup>P. J. Mulders, A. T. Aerts, and J. J. De Swart, *ibid.* **D 21**, 2653 (1980).
- <sup>38</sup>V. A. Matveev and P. Sorba, Nuovo Cimento **A 115**, 217 (1978).
- <sup>39</sup>I. Yu. Kobzarev, B. V. Martem'yanov, and M. G. Shchepkin, Yad. Fiz. **29**, 1620 (1979) [Sov. J. Nucl. Phys. **29**, 831 (1979)].
- <sup>40</sup>L. A. Kondratyuk, M. I. Krivoruchenko, and M. G. Shchepkin, Pis'ma Zh. Eksp. Teor. Fiz. **45**, 10 (1986) [JETP Lett. **45**, 10 (1987)].
- <sup>41</sup>L. A. Kondratyuk, M. I. Krivoruchenko, and M. G. Shchepkin, Yad. Fiz. **45**, 1252 (1987) [Sov. J. Nucl. Phys. **45**, 776 (1987)].
- <sup>42</sup>W. Kwong, J. L. Rosner, and C. Quigg, Ann. Rev. Nucl. Part. Sci. **37**, 325, 1987.
- <sup>43</sup>A. A. Bykov *et al.*, Usp. Fiz. Nauk **143**, 3 (1984) [Sov. Phys. Usp. **27**, 321 (1984)].
- <sup>44</sup>E. Eichten and F. L. Feinberg, Phys. Rev. **D 23**, 2724 (1981).
- <sup>45</sup>D. Gromers, Z. Phys. **C 26**, 401 (1984).
- <sup>46</sup>Pantaleone and S. H. Tye, Phys. Rev. **D 37**, 3337 (1988).
- <sup>47</sup>Yu. A. Simonov, Nucl. Phys. **B 307**, 512 (1988).
- <sup>48</sup>N. G. Dosch and Yu. A. Simonov, Phys. Lett. **B 205**, 339 (1988).
- <sup>49</sup>M. I. Krivoruchenko, Pis'ma Zh. Eksp. Teor. Fiz. **38**, 146 (1983) [JETP Lett. **38**, 173 (1983)].
- <sup>50</sup>M. G. Shchepkin, Yad. Fiz. **53**, 279 (1991) [Sov. J. Nucl. Phys. **53**, 177 (1991)].
- <sup>51</sup>C. Daum *et al.*, Nucl. Phys. **B 187**, 1 (1981).
- <sup>52</sup>Sh. S. Eremyan and A. E. Nazaryan, Yad. Fiz. **49**, 823 (1989) [Sov. J. Nucl. Phys. **49**, 512 (1989)].
- <sup>53</sup>J. Iizuka *et al.*, Phys. Rev. **D 39**, 3357 (1989).
- <sup>54</sup>V. Gupta and R. Kogerler, Z. Phys. **C 41**, 277 (1988).
- <sup>55</sup>M. G. Olson and C. J. Suchyta, Phys. Rev. **D 35**, 1738 (1987).
- <sup>56</sup>N. Isgur and G. Karl, *ibid.*, **D 18**, 4187 (1978).
- <sup>57</sup>N. J. Schnitzer, Preprint BRX TH-269, 1989.
- <sup>58</sup>A. B. Kaïdalov and A. V. Nogteva, Preprint ITEP-28, Moscow, 1987.
- <sup>59</sup>L. A. Kondratyuk, B. V. Martem'yanov, and M. G. Shchepkin, Yad. Fiz. **47**, 1747 (1988) [Sov. J. Nucl. Phys. **47**, 1107 (1988)].
- <sup>60</sup>A. Casher, H. Neuberger, and S. Nussinov, Phys. Rev. **D 20**, 179 (1979).
- <sup>61</sup>J. Schwinger, *ibid.* **82**, 664 (1951).
- <sup>62</sup>I. Yu. Kobzarev, B. V. Martem'yanov, and M. G. Shchepkin, Yad. Fiz. **48**, 541 (1988) [Sov. J. Nucl. Phys. **48**, 344 (1988)].
- <sup>63</sup>M. Abramowitz and I. A. Stegun (eds.), *Handbook of Mathematical Functions*, National Bureau of Standards, Washington, D.C., 1965 [Russ. transl., Nauka, M., 1979].

Translated by S. Chomet